CHALMERS
UNIVERSITY OF TECHNOLOGY

Ray-tracing Based Atmospheric Propagation Simulator for a 2x2 LOS MIMO System

Master thesis in Communication Engineering

YONGAN ZHOU

DEPARTMENT OF SPACE, EARTH, AND ENVIRONMENT
CHALMERS UNIVERSITY OF TECHNOLOGY
Gothenburg, Sweden 2023
www.chalmers.se

MASTER THESIS 2023

Ray-tracing Based Atmospheric Propagation Simulator for a 2x2 LOS MIMO System

YONGAN ZHOU

Department of Space, Earth, and Environment
CHALMERS UNIVERSITY OF TECHNOLOGY
Gothenburg, Sweden 2023

Ray-tracing Based Atmospheric Propagation Simulator for a 2x2 LOS MIMO System
YONGAN ZHOU

Supervisor: Lei Bao, Mikael Coldrey, Ericsson AB
Examiner: Patrick Eriksson, Department of Space, Earth, and Environment

Master Thesis 2023
Department of Space, Earth, and Environment
Chalmers University of Technology
SE-412 96 Gothenburg
Sweden
E-mail zya1937@outlook.com

Typeset in LaTeX
Gothenburg, Sweden 2023

Ray-tracing Based Atmospheric Propagation Simulator for a 2x2 LOS MIMO System
YONGAN ZHOU
Department of Space, Earth and Environment
Chalmers University of Technology

Abstract

A microwave radio system with multiple antennas is one popular technology for backhaul network deployment to reach the capability increase required for 5G and 6G. Antenna separations at transmit and receive sites should be carefully designed to ensure a proper phase relation, in this Multiple Input Multiple Output (MIMO) system with long Line-of-Sight (LoS) paths between transmitter and receiver. The LOS MIMO system may fail to operate under an extremely refractive atmosphere due to a lack of sufficient system gain which is determined by the power level and phase condition of the received sub-streams.

The contribution of the thesis is to provide a simulator that can model radio's atmospheric propagation, and it can be further used to verify real link measurement data. It is tested that the simulator has minor accuracy loss over the propagating distance concerned in this study. The simulation of electromagnetic wave propagation is based on Forward Ray Tracing (FRT). The results demonstrate that the simulator is capable of predicting channel performance (MIMO gain, MIMO phase, etc.) for a 2-by-2 LOS MIMO system over a refractive atmosphere. The results also demonstrate that the simulator is found to be in good agreement with the literature and with Parabolic Equation (PE) methods, validating its potential use for predicting the outage probability for the MIMO link.

This study, to the author's best knowledge, is the first work that models the impact of atmospheric refractivity on LOS MIMO channels using FRT. It is found that for a 2x2 LOS MIMO system the antenna separation calculated assuming free space propagation is also valid for the case of standard refractivity. For other refraction conditions, the link will more likely experience an outage due to variation in phase condition than loss of power. In addition, atmospheric multipath may induce random MIMO phase variation. However, the simulator cannot yet properly tackle surface-induced effects on the signals; this requires further development of the software.

Keywords: Line-of-Sight, radio propagation, troposphere duct, wireless backhaul, atmospheric refraction, microwave link planning.

Acknowledgements

The author would like to thank research manager Henrik Sahlin for providing this job opportunity; the author would like to thank senior researcher Lei Bao and principal researcher Mikael Coldrey for their tutoring and documents that helped me understand the project and relevant technical details; the author would like to thank professor Patrick Eriksson for providing ARTS theory book and relevant code to study, which accelerates the whole project accomplishment.

The above thanks are in no particular order and are weighted equally.

Professor Patrick and researcher Lei provided a great many suggestions and comments regarding this report, the author would like to express his gratitude for their time and patience.

Finally, a special thanks to my parents who are always supporting and caring for me even though they are hemisphere away.

Yongan Zhou, Gothenburg, August 2023

Contents

1

Introduction

1.1 Background

Microwave links are a type of wireless communication technology that uses high-frequency radio waves to establish connections between two or more locations. Microwave links are commonly used for point-to-point communication in various applications, including satellite, and backhaul for mobile networks.

Wireless backhaul refers to the use of microwave links to connect two or more network nodes. It is a popular option for mobile network operators. One advantage of wireless backhaul is its flexibility in providing high-speed connectivity to remote and difficult-to-reach areas. Wireless backhaul links also enable transmission of large amounts of data over long distances (e.g., over 45 km), to support the increasing demand for data traffic generated by mobile devices.

Microwave links require a clear Line-of-Sight (LOS) path between the transmitting and receiving antennas. Each microwave link should ensure an outage probability of less than 0.01% - 0.001% of a year. This requirement determines the transmission distance (referred to as hop length) for a given frequency. Outage prediction should include several types of fading events: rain, frequency selective fading, and non-frequency selective fading (also referred to as flat fading). Raindrops, ice, and snow are capable of inducing absorption and scattering effects on microwave signals, leading to a degradation of received signal strength. Atmospheric refraction and air turbulence may cause coherent/incoherent variation of channel frequency response concerning symbol bandwidth, leading to flat fading and selective fading.

Multiple antenna technology can be integrated into high-frequency microwave radio links. It is common to refer to this kind of system as a LOS MIMO (Multiple-Inputs-Multiple-Outputs) system [1]. However, LOS links are subject to atmospheric-induced channel variation. International Telecommunication Union (ITU) has published a series of prediction methods for the design of terrestrial Line-of-Sight single antenna systems [2], but there are no ITU recommendations for spatially separated MIMO links. For high-frequency and short MIMO links, previous field measurements observed that rain fading induces almost fully correlated power attenuation and minor phase variation. On the other hand, long-haul MIMO links at lower frequencies are mostly affected by refractivity-induced flat fading where the impact of refractivity on the signal phase is rarely studied. A proper phase relation between transmitter and receiver is crucial for ensuring link availability, yet there is a lack of literature and field measurement regarding this topic, therefore availability prediction of flat fading for long MIMO links is a challenging research topic.

To address atmospheric refractivity-induced channel variation, both Forward Ray Tracing (FRT) and Parabolic Equation (PE) models are worth investigating. FRT follows the photon's path from the radiation source to the receiver, it computes propagation paths using 3-D/2-D geometry [3]. Another ray tracing technique is Backward Tracing, which is not used in this study. In contrast, it follows a ray from the receiver backward to the transmitter. In the scope of this study, two terms (RT/FRT) are exchangeable since there is no practical difference here in going forward or backward. PE model is an alternative approach to the solution of radio wave propagation modeling. The parabolic equation method divides the propagation region into a series of vertical/horizontal slices, and the wave equation is solved for each slice by utilizing the finite-difference methods or Fourier transforms [4][5].

In the study, an RT-based model is developed to track the signal and calculate how it is affected by the refractive atmosphere. Thereafter, such a model will be integrated into a 2x2 LOS MIMO channel matrix to simulate the atmospheric impact on the radio channel. Finally, simulated results will be verified by comparing them with published literature and work from another research team, validating model's capabilities of predicting MIMO performance via ARTS theories [3].

1.2 Objectives

The aim of this thesis is as follows.

- Ray tracing-based simulation of SISO and MIMO radio channel for both power/phase prediction under both normal/abnormal refractivity profiles.
- Prediction of key metrics of LOS MIMO system performance under both normal/abnormal refractivity profile.

1.3 Limitations / Demarcations

- Apart from atmospheric refractivity, terrain factors, such as surface reflection and diffraction, play an essential role in affecting the signal's trajectory. In this study, the primary goal is to model a pure atmospheric propagation, under the assumption of flat terrain.
- The atmosphere is assumed to be stratified, meaning the weather parameters are only altitude-dependent, and refractivity is invariant along a horizontal direction. In the study, it considers the same profile regardless of the distance to the antenna.
- Concerning turbulence, the corresponding time scale is assumed to be negli-

gible compared to the symbol duration and travel time. Hence, the impact of turbulence is not included in the model/study.

- Defocusing caused by extremely refractive layers in the atmosphere must be taken into account in the planning of links of more than a few kilometers in length [2]. However, the emphasis of this thesis is to predict the signal's phase under extreme refractivity, which is rarely studied. Therefore defocusing/beam spreading is neglected, given numerous researches that have already been conducted regarding this fading mechanism.

1.4 Thesis Outline

Chapter two gives a basic introduction to the theoretical background regarding LOS MIMO, atmospheric propagation, FRT, and radio propagation. Chapter three focuses on the numerical implementation of a 2x2 LOS MIMO channel affected by atmospheric refractivity, and it describes the essential workflow of the RT simulator. Additionally, necessary simplifications and assumptions are also presented. Chapter four shows the verification of a ray-tracing based 2x2 LOS MIMO simulator. A series of simulation goals, experimental setup, simulation results, and result analysis are presented. Chapter five concludes the overall work; discusses limitations/shortage of thesis work; and gives a future outlook.

2

Theory

The purpose of this chapter is to give the theoretical knowledge required for implementing the FRT-based simulator. Section 2.1 describes a 2x2 LOS MIMO in free space where atmospheric refraction is absent. Section 2.2 describes the basic treatment of atmospheric refraction. Section 2.3 describes how atmospheric refractivity would affect the radio signal.

2.1 Line of Sight MIMO

LOS MIMO refers to a wireless communication system that utilizes multiple antennas at both the transmitter and receiver side, with an unobstructed direct line-of-sight path between every pair of transmitter and receiver antennas.

In actual deployment, the reliability of such a system is subject to atmospheric and terrestrial conditions. According to previous outdoor measurements for several LOS MIMO trial links of relatively short length [6], the short links (but high frequency, e.g., 32 GHz) are mainly affected by rain fading, whilst the impact of multipath fading is minor. The rain fading (power attenuation) estimation can follow the current ITU-R P530 specification [2].

LOS MIMO long haul link considered in this study is at lower frequencies, with mid-range/long hop length (e.g., 6 GHz, over 40 km), and is mainly affected by refractivity-induced flat fading. It is shown from measurements, that due to a large change in signal phase, an outage can happen even if the power level is sufficiently good.

2.1.1 Channel Matrix

Mathematically, the relation between the transmitted signals from multiple antennas at the transmitter and the received signals at multiple antennas at the receiver can be described by a channel matrix.

In a radio access network, MIMO communication between the base station and user equipment, it is common that the number of transmit antennas can be different from the number of receiver antennas [7].

In wireless backhaul applications, the bi-directional links are typically equipped with the same number of transmit and receive antennas.

Here the 2x2 MIMO channel matrix can be represented by:

$$\mathbf{H} = \begin{bmatrix} h_{11} & h_{12} \\ h_{21} & h_{22} \end{bmatrix} = \begin{bmatrix} a_{11}e^{j\Phi_{11}} & a_{12}e^{j\Phi_{12}} \\ a_{21}e^{j\Phi_{21}} & a_{22}e^{j\Phi_{22}} \end{bmatrix} \tag{2.1}$$

where:

a_{nm} represents the channel gain (no units) of sub-stream h_{nm} from n_{th} transmit antenna to m_{th} receive antenna;

Φ_{nm} represents the phase shift (radian) of sub-stream h_{nm} from n_{th} transmit antenna to m_{th} receive antenna;

Considering the vacuum where rays travel along a straight path, the optical path length for a transmitted symbol would be the geometrical distance between a TX (transmitter) antenna and an RX (receiver) antenna.

By assuming equally received power (normalized to 1) [4], Equation 2.1 can be rewritten as:

$$\mathbf{H_{LOS}} = \begin{bmatrix} e^{j\frac{2\pi}{\lambda}d_{11}} & e^{j\frac{2\pi}{\lambda}d_{12}} \\ e^{j\frac{2\pi}{\lambda}d_{21}} & e^{j\frac{2\pi}{\lambda}d_{22}} \end{bmatrix} \tag{2.2}$$

where:

d_{nm} is the geometrical distance(meter) between n_{th} transmitting antenna to m_{th} receiving antenna.

λ is the wavelength (meter).

2.1.2 Spatial Multiplexing

Spatial Multiplexing is a technique that enables increased data rates and enhances spectral efficiency. The serial data symbols will be divided into several sub-streams by pre-processing, the transmitter then maps different symbols or data streams onto the spatially separated transmit antennas. Multiplexed data is carried by these transmit antennas, exploiting different propagation paths. At the receiver, the multiple receive antennas capture the mixed signals, and through signal processing algorithms, e.g., zero forcing cancellation, the receiver cancels out the interference data streams and recovers the desired data stream [8].

The received symbol for a 2x2 MIMO can be written as:

$$\begin{bmatrix} y_1 \\ y_2 \end{bmatrix} = \begin{bmatrix} a_{11}e^{j\Phi_{11}} & a_{12}e^{j\Phi_{12}} \\ a_{21}e^{j\Phi_{21}} & a_{22}e^{j\Phi_{22}} \end{bmatrix} \begin{bmatrix} x_1 \\ x_2 \end{bmatrix} + \begin{bmatrix} n_1 \\ n_2 \end{bmatrix} \tag{2.3}$$

or Equation 2.3 can be written in the matrix form considering the LOS scenario:

$$\mathbf{y} = \mathbf{H_{LOS}}\mathbf{x} + \mathbf{n} \tag{2.4}$$

where:

$\mathbf{n}$ is the noise vector, which comprises independently Gaussian distributed noise elements n_1 and n_2;

$\mathbf{x}$ is the transmitted symbol vector, which contains x_1 and x_2;

$\mathbf{y}$ is the received symbol vector, which contains y_1 and y_2.

2.1.3 Singular Value Decomposition (SVD)

If the channel condition (i.e., channel matrix) is known at both the transmitter and receiver sides, the transmitter and receiver can precode/equalize the signals to achieve the highest possible data rate and to separate independent data streams.

SVD decomposes the original channel into several parallel sub-channels. The number of sub-channels is equal to the rank of the decomposed channel, which also corresponds to the minimum number between transmitting antennas N_t and receiving antenna N_r.

For the LOS MIMO link in this study, $N_r = N_t = N$.

A complex N by N channel matrix can be decomposed by SVD into:

$$\mathbf{H} = \mathbf{U}\boldsymbol{\Sigma}\mathbf{V}^H \tag{2.5}$$

where:

$\mathbf{U}^H$ is a N by N unitary equalizer matrix, $(\cdot)^H$ denotes Hermitian transpose;

$\boldsymbol{\Sigma}$ is a N by N diagonal matrix, it yields $\boldsymbol{\Sigma} = \mathrm{diag}(\sigma_1, \ldots, \sigma_N)$, σ is the singular value;

$\mathbf{V}$ is an N by N unitary precoder matrix.

Assuming data symbols are denoted by $\mathbf{x}$, it becomes $\mathbf{Vx}$ after precoding. The recovered symbol z, after equalizing, can be expressed as:

$$\begin{aligned}
\mathbf{z} &= \mathbf{U}^H\mathbf{y} \\
\mathbf{z} &= \mathbf{U}^H(\mathbf{HVx} + \mathbf{n}) \\
\mathbf{z} &= \mathbf{U}^H\mathbf{U}\boldsymbol{\Sigma}\mathbf{V}^H\mathbf{Vx} + \mathbf{U}^H\mathbf{n} \\
\mathbf{z} &= \boldsymbol{\Sigma}\mathbf{x} + \mathbf{w}
\end{aligned} \tag{2.6}$$

The advantage of the SVD technique is a simple signal detector at the receiver side because $\boldsymbol{\Sigma}$ is diagonal. It avoids noise enhancement problems because a unitary matrix does not scale the noise power. In this case, $\mathbf{w}$ is the rotated noise vector.

2.1.4 Condition Number

The ratio of the maximum singular value and the minimum one is the channel's condition number κ, it describes how ill-conditioned the channel is:

$$\kappa(\mathbf{H_{LOS}}) = \frac{\sigma_{\max}}{\sigma_{\min}} \tag{2.7}$$

If a 2x2 MIMO channel is well conditioned, two sub-streams in the LOS MIMO should have two equal corresponding singular values σ_1 and σ_2 from $\mathbf{\Sigma}$. At optimal antenna separation, the MIMO channel has a condition number of one. If antennas were not spatially separated optimally, channel decomposition would give a condition number greater than one.

2.1.5 MIMO Phase and Antenna Separation

For a normalized 2x2 LOS MIMO matrix where its element has unit power, the capacity is maximized as the diagonal values of $\mathbf{\Sigma}$ are equal. In this case, the inner product between any two streams that are transmitted by the same antenna in the $\mathbf{H_{LOS}}$ is equal to zero:

$$\langle h_k, h_l \rangle = \sum_{n=1}^{N} e^{j(\angle h_{nk} + \angle h_{nl})} = 0 \tag{2.8}$$

The orthogonality in the signal space gives termination of cross-talk and the phase difference between MIMO paths in this case should ideally be 0 degree [9]:

$$\theta_{MIMO,optimal} = 180^o - ((\angle h_{12} - \angle h_{11}) + (\angle h_{21} - \angle h_{22})) = 0^o \tag{2.9}$$

where:

$\angle h_{nm}$ corresponds to $e^{j\phi_{nm}}$ in Equation 2.2.

An analytical expression of the line-of-sight MIMO phase (no refraction) can be written as:

$$\theta_{MIMO} = 180^o - 2(\sqrt{(R+d)^2} - R)(\frac{2\pi}{\lambda})(\frac{180^o}{\pi}) \tag{2.10}$$

where:

R is the hop length (meter);

d is the antenna separation (meter).

Assuming the antenna separation at TX and RX sides vary simultaneously by a same amount, solving Equation 2.10 concerning d:

$$d_{optimal} = \sqrt{\frac{\lambda R}{N}} \tag{2.11}$$

2.1.6 MIMO Gain

MIMO gain is the enhancement/degradation in signal-to-noise ratio for the recovered signal compared to single-input single-output (SISO) systems. For cancellation-based 2x2 LOS-MIMO receiver which has equal received power (see Equation 2.2), the relative MIMO gain to SISO can be described as following LOS-MIMO Power Enhancement Factor (PEF) [9]:

$$PEF = 20\log_{10}\left(2\left|\sin\left(\frac{\pi}{2} - \frac{\theta_{MIMO}}{2}\frac{\pi}{180^o}\right)\right|\right) - 10\log_{10} 2 \tag{2.12}$$

Under the optimal antenna separation besides $\theta_{MIMO} = 0^o$:

$$PEF_{optimal} = 20\log_{10}\left(2\left|\sin\left(\frac{\pi}{2}\right)\right|\right) - 10\log_{10} 2 = 3.01^{[\mathrm{dB}]} \tag{2.13}$$

LOS MIMO system gives maximum MIMO power enhancement when the antennas are placed at optimal antenna separation, while a system outage could happen when antennas are closely separated. Typically, a microwave link (SISO) has a typical 30-40 dB fading margin (see section 2.4.4). In the MIMO case, there is an additional loss due to the sub-optimal phase relation between TX and RX, see Figure 2.1.

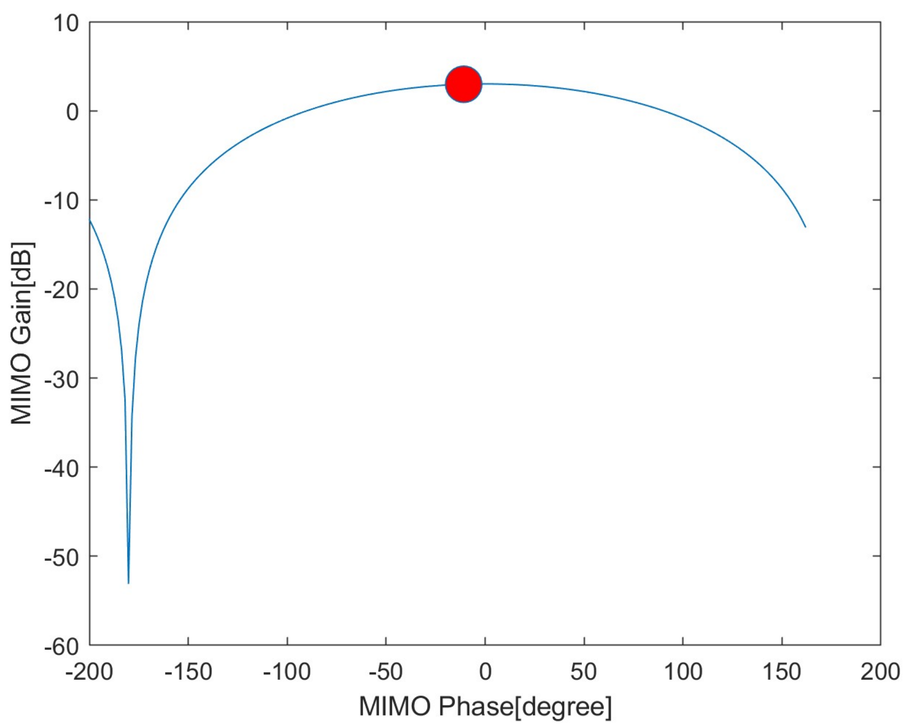

Figure 2.1: For cancellation-based LOS-MIMO receivers, PEF is a function of the MIMO phase. Compared to SISO, approximate 3 dB MIMO gain is due to the signal from one transmit antenna being received at two receive antennas. PEF is less than 3 dB as the antenna is not optimally separated.

The above system description is based on a simple assumption that the radio signal travels in a straight line between TX and RX antennas. Trial measurement of long links showed that the simple assumption will not work during certain atmospheric conditions, therefore it is desired to model the impact and perform quantitative analysis.

2.2 Atmospheric Refractivity

Atmospheric refraction is the bending and the delay of radio waves as they pass through the Earth's atmosphere. This phenomenon is modeled by the variation in the refractive index of the atmosphere, which changes with temperature, pressure, and humidity.

Refractivity index, designated as n, can be modeled as a function of meteorological parameters [10]:

$$n = 1 + \left(77.6\frac{P}{T} - 5.6\frac{e}{T} + 3.75 \times 10^5 \frac{e}{T^2}\right) \times 10^{-6} \qquad (2.14)$$

where:

P is the atmosphere pressure in millibars;

T is the atmosphere temperature in Kelvin;

e is the water vapour pressure.

Another way to express the refractivity of the atmosphere is Radio Refractivity N (N unit):

$$N = (n - 1) \times 10^6 \qquad (2.15)$$

The modified refractivity profile M (M unit) can be computed based on the profile of meteorological parameters according to the following formula:

$$M = N + 0.157z \qquad (2.16)$$

where:

z is the height (meter) above some reference, usually the earths surface.

2.2.1 Atmospheric Refraction of Radio Signal

In the presence of atmospheric refraction, radio waves can be bent towards the Earth's surface, causing them to propagate along curved trajectories. For example, atmospheric refraction can cause radio signals to be received beyond the radio horizonline of sight, which is the point at which radio signals should no longer be able to be received.

The gradient of atmospheric refractivity can decide how the signal is bent. Based on towards which direction the signal is bent and how intense the bending is observed, four typical refractive condition types are defined in Table 2.1.

Table 2.1: Refractive condition type [4].

Refraction Type	dN/dz (N units/km)	dM/dz (M units/km)
Sub	> -39	> 118
Normal	= -39	= 118
Super	< -39	< 118
Ducting/Trapping	< -157	<0

In Figure 2.2, in the sub-refraction case, the radio signal is bent upwards and the energy travels away from the surface. In the super refraction case where the refractivity gradient is negative, the radio signal is bent downwards and it can be trapped and travel a very long distance if the gradient is strongly negative (trapping/ducting).

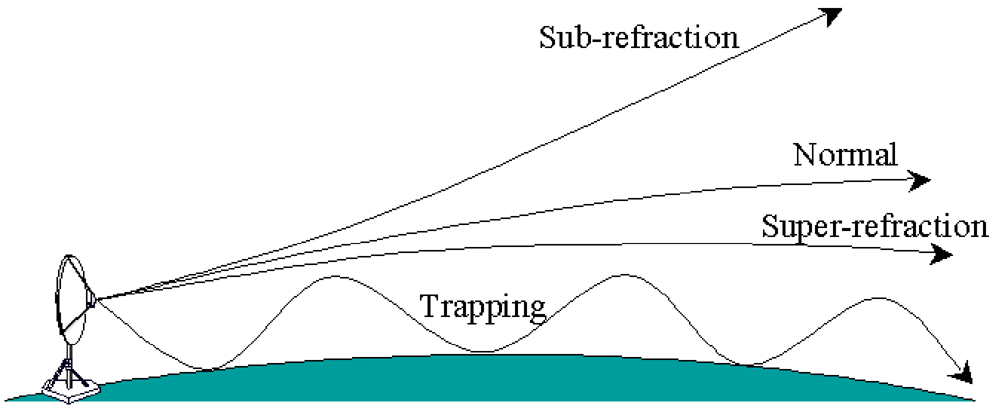

Figure 2.2: Four types of refraction [11].

The refractivity index n (see Equation 2.14) in the atmosphere is different from that in a vacuum and varies in the height direction. Table 2.1 gives the ranges in which the refractivity gradient describes refractive conditions. In Figure 2.3, depending on the inversion layer's thickness and position, it can be further modeled into surface duct, surface-based duct, and elevated duct.

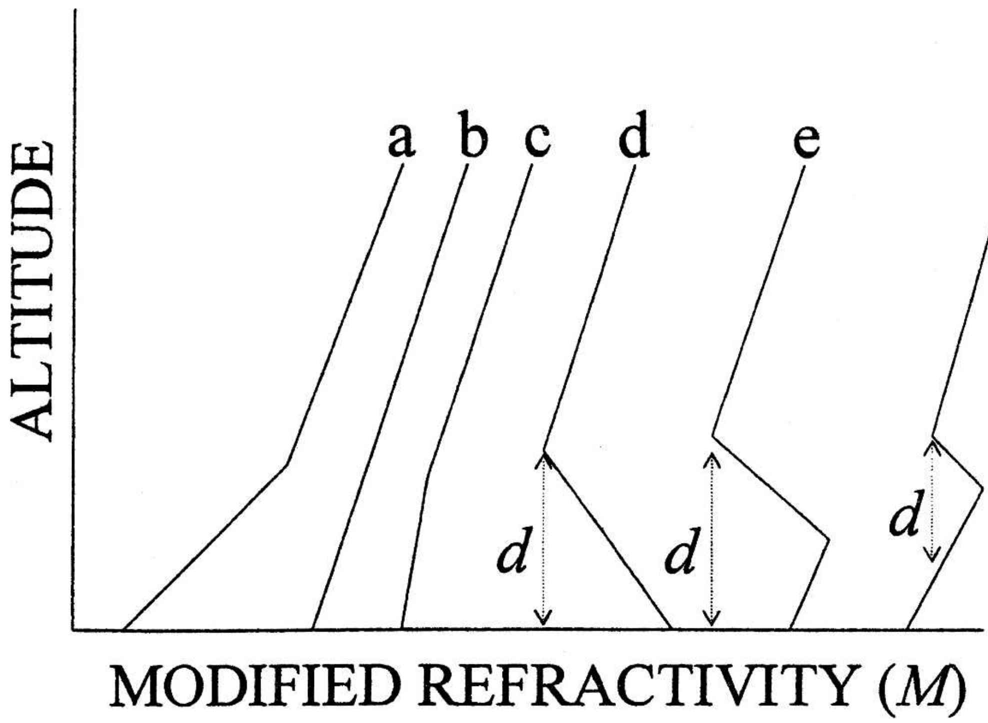

Figure 2.3: (a) sub-refraction, (b) standard, (c) super-refraction, (d) surface duct, (e) surface-based duct, (f) elevated duct [12].

These inversions typically occur due to the advection of dry, warm air over the Earths surface, which may be over both ocean and land, leading to sharp humidity and temperature inversions or making moist air trapped between cooler layers [12].

Atmospheric ducting is of particular interest to radio communication systems, including marine and aviation communication, long-range radio broadcasting, and over-the-horizon radar. Understanding and predicting ducting conditions can help optimize system performance and mitigate the potential degradation of this phenomenon.

2.3 Ray Optics

2.3.1 Snell's Law

Snell's law, also known as the law of refraction, describes the relationship between the angles of incidence and refraction when a light ray passes through the boundary between two different media, such as air and water or air and glass. It states:

$$n_1 \sin \phi_1 = n_2 \sin \phi_2 \tag{2.17}$$

where:

ϕ_1 and ϕ_2 are the incident angle (radian) and refracted angle (radian).

n_1 and n_2 are the refractivity indices of the homogeneous media.

This phenomenon is also associated with a changing speed of light as ray travels through different media:

$$v_1 \sin \phi_2 = v_2 \sin \phi_1 \tag{2.18}$$

where:

v_1 and v_2 are the wave velocities (m/s) through the respective media, it yields $v_i = c/n_i$.

2.3.2 Forward Ray Tracing

The Recommendation ITU R P.676-10 considers the atmosphere as being divided into spherical homogeneous layers [14], each layer has a constant refractivity index. A ray follows a straight trajectory in each layer, and the ray's new direction is recalculated when it crosses layers. A ray travels through different homogeneous layers, the ray is advanced by a small amount.

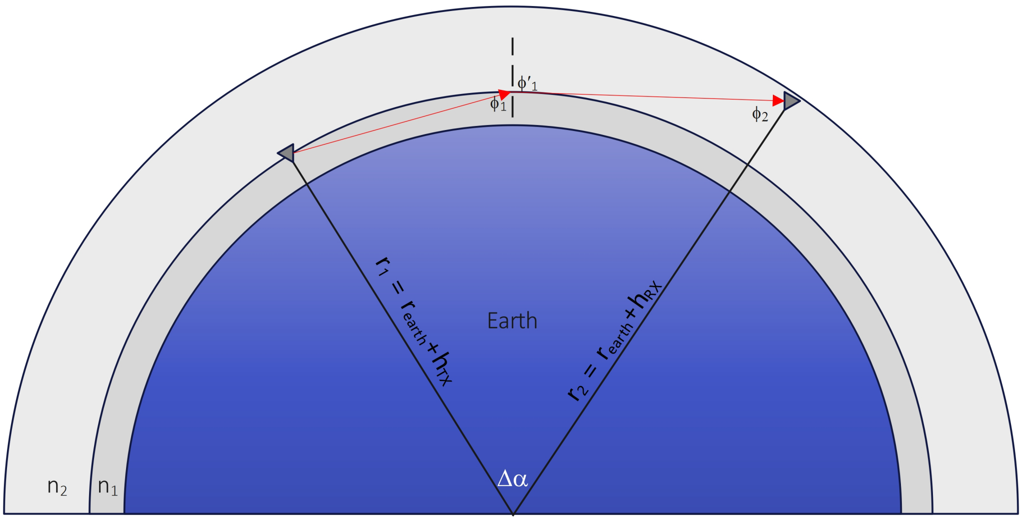

Figure 2.4: Ray propagates in spherical homogeneous media.

From the boundaries of each layer, a ray segment's new direction can be traced by applying Snell's law. In each layer, a new segment is sent out and the process is repeated until a complete path is generated.

Applying Snells law in Figure 2.4 gives:

$$n_1 \sin(\phi_1) = n_2 \sin(\phi\prime_1) \tag{2.19}$$

And the law of sine gives:

$$\frac{\sin(\phi_2)}{r_1} = \frac{\sin(\phi\prime_1)}{r_2} \tag{2.20}$$

By combining both equations:

$$p_c = r_1 n_1 \sin(\phi_1) = r_2 n_2 \sin(\phi_2) \tag{2.21}$$

where:

p_c is the path constant, i.e., a constant along the propagation path.

r_1 and r_2 is wave's current radical coordinate to Earth center;

For each layer, a ray segment's next direction is given by inversion of the sine function:

$$\phi_{i+1} = \arcsin(r_i n_i / p_c) \tag{2.22}$$

Alternatively, the bending of a ray's trajectory can be described by how much it deviates from how it is in the vacuum or uniform mediathe amount of the deviation along the path s is represented by ϵ in Figure 2.5:

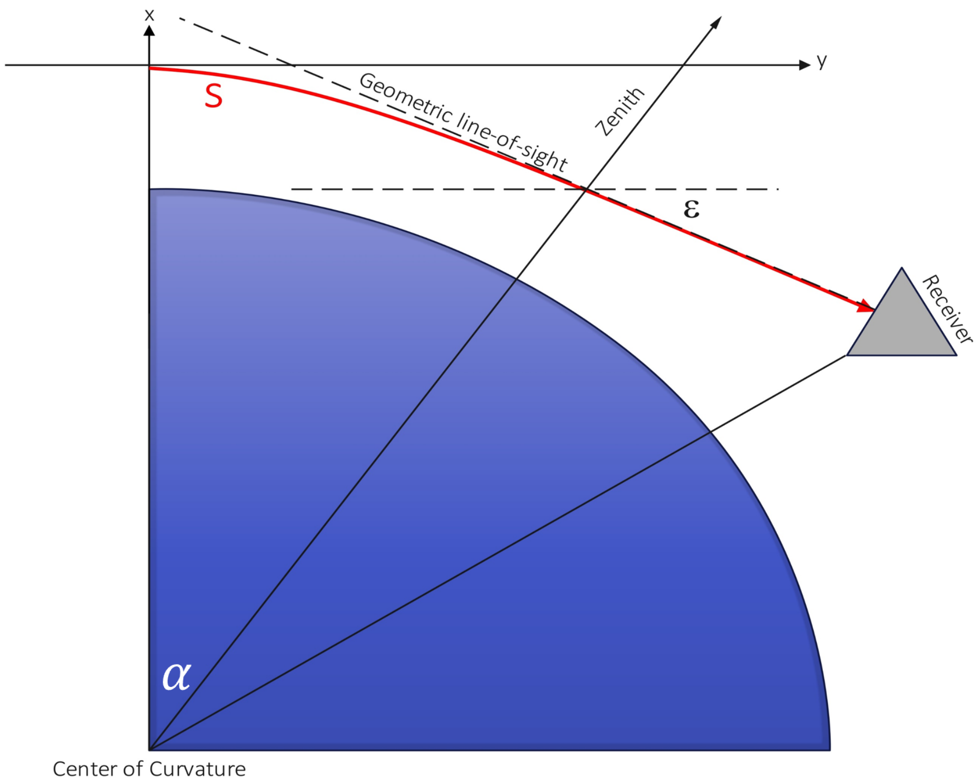

Figure 2.5: A bent ray's path in refractive media, α is ray's current angular coordinate in the polar coordinates.

A differential equation of ϵ with respect to s describes ray's trajectory [15]:

$$\frac{\mathrm{d}\epsilon}{\mathrm{d}s} = \frac{1}{n}\left(\frac{\partial n}{\partial \bar{t}}\right)_{\epsilon} \tag{2.23}$$

where:

ϵ is ray's direction with respect to horizon/x axis in Cartesian system;

$\bar{t}$ is coordinate perpendicular to ϵ;

n is the refractivity index at ray's current position.

Mapping $\bar{t}$ to Cartesian coordinates system:

$$\left(\frac{\partial n}{\partial \bar{t}}\right)_{\epsilon} = -\sin\epsilon\left(\frac{\partial n}{\partial y}\right)_{x} + \cos\epsilon\left(\frac{\partial n}{\partial x}\right)_{y} \tag{2.24}$$

Equation 2.23 becomes:

$$\frac{\mathrm{d}\epsilon}{\mathrm{d}s} = -\frac{\sin\epsilon}{n}\left(\frac{\partial n}{\partial y}\right)_{x} + \frac{\cos\epsilon}{n}\left(\frac{\partial n}{\partial x}\right)_{y} \tag{2.25}$$

Expressing Equation 2.25 into polar coordinates if spherical layers are considered[5]:

$$\frac{\mathrm{d}(\phi+\alpha)}{\mathrm{d}s} = -\frac{\sin\phi}{n}\left(\frac{\partial n}{\partial r}\right)_{\alpha} + \frac{\cos\phi}{nr}\left(\frac{\partial n}{\partial \alpha}\right)_{r} \tag{2.26}$$

where:

α and r are angular coordinate (radian) and radial coordinate respectively;

ϕ is the angle (radian) between the zenith and the ray's tangent.

Following Figure 2.4, considering horizontally homogeneous media where refractivity is only altitude dependent:

$$\frac{\mathrm{d}(\phi)+\mathrm{d}(\alpha)}{\mathrm{d}s} = -\frac{\sin\phi}{n}\left(\frac{\partial n}{\partial r}\right)_{\alpha} \tag{2.27}$$

To make the formula accessible to the computer, it must be converted to discrete form:

$$\frac{(\phi_{i+1}-\phi_i)+(\alpha_{i+1}-\alpha_i)}{l_g} = \frac{1}{n_i}\cdot -\sin\phi_i\frac{dn}{dz} \tag{2.28}$$

where:

l_g is the step length of ray's segment, corresponds to ds in continuous case;

$\frac{dn}{dz}$ is the vertical gradient of refractivity profile.

The geometrical zenith angle at ray tracing iteration i+1 is [3]:

$$\phi_{i+1} = \phi_i - (\alpha_{i+1}-\alpha_i) + \frac{l_g}{n_i}\left[-\sin\phi_i\left(\frac{dn}{dz}\right)\right] \tag{2.29}$$

2.3.3 Optical Path Length

Optical path length (OPL) refers to the distance that light travels through a medium or an optical system [16]. It is the cumulative distance that light needs to travel through the air to create the same phase difference as it would have when traveling through some uniform medium or vacuum.

In layered atmosphere [17], OPL is calculated by taking the product of the distance ray advances in each layer and the refractive index of the homogeneous layer through which the ray propagates. For inhomogeneous media, the thickness of each layer is inclined to an infinitesimal number, and OPL is calculated by a line integral of the refractivity index along the ray path:

$$OPL = \int_C n(s)\mathrm{d}s. \tag{2.30}$$

For such cases it is continuously varying refractive media light travels in, $n(s)$ is the local refractivity index which changes along ray's path s.

2.4 Radio Propagation

2.4.1 Antenna Radiation Pattern

An antenna's electromagnetic wave radiation or reception in three dimensions is represented graphically by the antenna radiation pattern. It displays the received signal intensity or radiated power spatial distribution as a function of direction with respect to the antenna. The azimuth plane (H plane) and the elevation plane (V plane) are useful for measuring and visualizing an antenna's radiation pattern. Two primary categories of radiation patterns exist:

- Omni-directional: An omni-directional antenna radiates or receives electromagnetic waves uniformly in all directions around it. In the azimuth plane, the radiation pattern appears as a circular shape. This type of pattern is common for antennas used in applications such as Wi-Fi routers, and cellular base stations.

- Directional: A directional antenna concentrates its radiation in specific directions while reducing power in other directions. In the azimuth plane, the radiation pattern appears as a series of lobes pointing in different directions. The main lobe is protuberant and provides the highest gain, allowing for longer-range communication in the desired direction. Directional antennas are commonly used in point-to-point microwave links, and satellite communication.

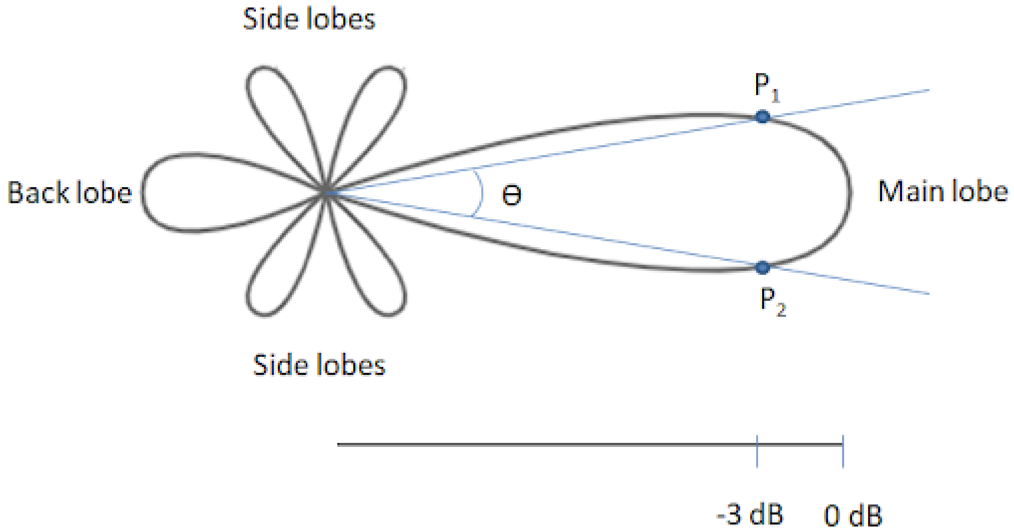

Figure 2.6: The radiation pattern of a directional antenna.

The θ in Figure 2.6 denotes the half-power beam width (HPBW). It is a measure of the angular width of the main lobe in the radiation pattern of an antenna. It represents the angular span between the points (P_1 or P_2) on the radiation pattern where the power or signal strength is half (-3 dB) of the maximum value in the main lobe.

For a parabolic antenna or dish antenna, the HPBW is given by [18]:

$$\theta = k\lambda/D \tag{2.31}$$

where:

λ is the wavelength (meter) of the electromagnetic wave it emits;

k is the feed illumination, usually 70 (degree) [18];

D is the dish diameter (meter).

2.4.2 First Fresnel Zone

In any wave-propagated transmission between a transmitter and receiver, most waves follow the direct line-of-sight path, while others propagate along a refracted or reflected path. In Figure 2.7, it is possible, however, for the signal to be reflected from objects that, although not in the direct/line-of-sight path, are captured by the receiving antenna if they are somehow close enough to the beamwidth [19]. Reflected signals are usually delayed and phase-shifted compared to direct ones because their OPL is longer. When the phase difference between them as they add up on the receiver side is half an odd integer of the period, destructive interference occurs.

The Fresnel zones are defined as an infinite number of concentric elliptical regions surrounding the direct line-of-sight (LOS) path, with the first Fresnel zone being the most important for practical purposes. In the first Fresnel zone, the distance from the transmitting antenna to each ring plus the distance from the ring to the receiving antenna is equal to one-half wavelength more than the direct path between the antennas [19].

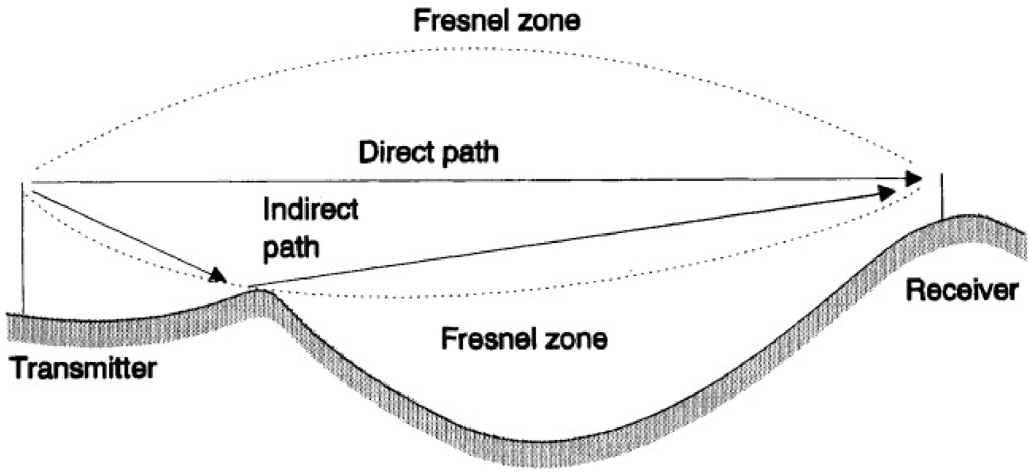

Figure 2.7: The Fresnel zone[20].

To maintain a direct path between the transmitter and receiver, the first zone must be kept largely free from obstructions/terrain. The radius of the first Fresnel zone at a point D_1 along the direct path of length R from the transmitting to the receiving antennas is :

$$r_1 = \sqrt{\frac{D_1 D_2 \lambda}{R}} \tag{2.32}$$

where:

r_1 is the radius (meter) of the first Fresnel zone;

D_2 is the distance (meter) from D_1 to the receiving antenna, $D_2 = R - D_1$

R is the total geometric line-of-sight distance (meter) between a pair of antennas.

2.4.3 Angle of Arrival

In the planning phase, antennas are pointed at a geometric line-of-sight direction where their antenna gain is maximized (main beam axis).

However, atmospheric refraction may make the signal approach the receiving antenna from a tilted angle w.r.t. bore-sight direction. In Figure 2.8, AoA (Angle of Arrival) is the angle between the incidence ray and the antenna's main beam axis. In this case, AoA is equal to the angle of azimuth/elevation relative to the main beam axis, considering the Gaussian beam (rotational symmetrical) in 2-D propagation.

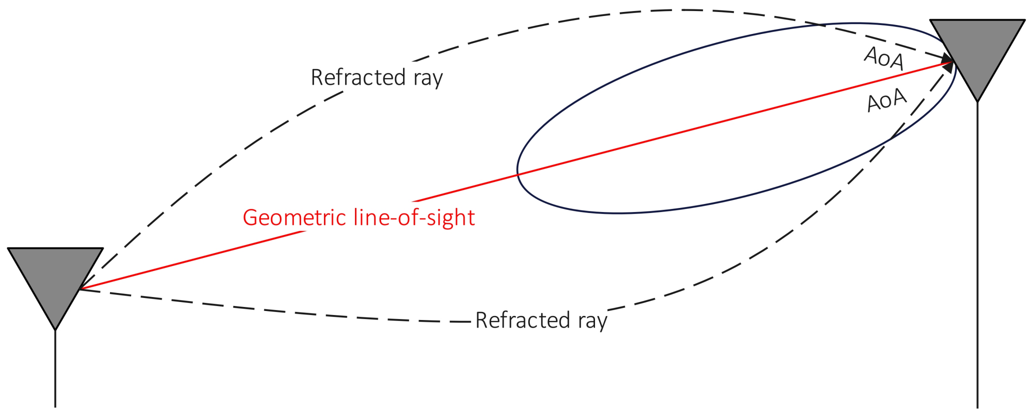

Figure 2.8: Tilted AoA.

The gain of the receiving antenna can be calculated according to the antenna pattern as exemplified in Figure A.1.

2.4.4 Channel Gain

Channel gain refers to the enhanced/reduced received signal power as it is compared with transmitted power. Received signal power of the microwave link, apart from free space path loss, can be mainly determined by rain attenuation, gaseous attenuation, and multipath fading. Gaseous absorption and rain attenuation, according to ITU, are the dominant fading types for higher carrier frequency, especially at millimeter-wave frequencies and higher (tens to hundreds of GHz) [14].

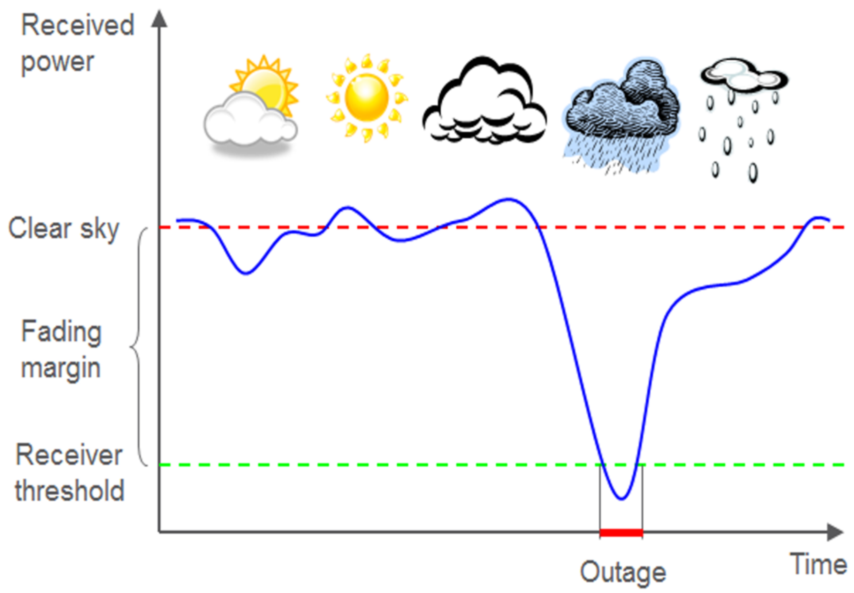

Figure 2.9: Received power degradation due to atmospheric activities, compared to clear sky.

In Figure 2.9, as received power degrades to the receiver threshold (minimum received power required), the system experiences an outage (no data throughput). Fading margin is defined as an interval from the received power level in the clear sky to the receiver threshold.

Assuming microwave planning ensures Fresnel zone clearance and the communication system operates below 10 GHz, therefore rain and gaseous attenuation are negligible. For one MIMO sub-stream (e.g., h_{nm}), the channel gain a is determined by free space pathloss which is given by Friis equation [21]:

$$a = \frac{P_r}{P_t} \approx G_t G_r \left(\frac{\lambda}{4\pi d}\right)^2 \tag{2.33}$$

where:

G_t is the gain of the transmitting antenna;

G_r is the gain of the receiving antenna;

d is the total propagation distance (m), in refractive atmosphere $d = OPL$;

Since the TX antenna and RX antenna are aligned during the installation, therefore G_t is maximized. According to section 2.4.3, the G_r relative to the main beam can be calculated according to AoA and the antennas radiation pattern in Figure A.1.

The multipath fading can be the result of both ground reflection and atmospheric inversion layers. Especially on long links, the strong gradient of the air refractivity index at a certain height may result in additional path length for radio waves to travel in it. At the RX antenna, multiple signal copies from the same TX antenna add up, which leads to multipath fading in most cases.

The multipath fading effect is the complex magnitude of the superposition of multipath copies:

$$|h| = |\sum_i a_i e^{j\Phi_i}| \tag{2.34}$$

Where:

Φ_i represents the phase of one of the signal's multipath copies.

2.4.5 Phase Shift

A propagated ray's phase in refractive media is a cumulative value of its travel distance:

$$\Phi(s) = \Phi(0) + \frac{2\pi}{\lambda_0}\int_C n(s)\mathrm{d}s \tag{2.35}$$

The total phase shift of a single ray is given by:

$$\Delta\Phi = 2\pi\frac{OPL}{\lambda_0} \tag{2.36}$$

where:

$\phi(0)$ is the initial phase (radian) of the ray;

λ_0 is the wavelength in vacuum (n = 1).

3

Methods

The numerical implementation of the atmospheric propagation for the LOS MIMO system is done with MATLAB and is guided by the ARTS theory book [3]. Section 3.1 describes how vertical refractivity profiles are modeled in MATLAB. Section 3.2 and Section 3.3 show a ray tracing workflow of tracking an electromagnetic wave until it is received. Section 3.4 gives the detailed implementation of a 2x2 LOS MIMO system.

3.1 Vertical Profile Modelling

This section describes how vertical refractivity profiles in Figure 2.3 are modeled in MATLAB.

Surface duct, (d) in Figure 2.3, can be modeled as a bi-linear function. Alternatively, a smooth function describing surface-based duct/elevated duct was described by [13]:

$$N = N_{\mathbf{0}} + kz + \frac{\Delta N}{\pi} \arctan \frac{[12.63(z - z_0)]}{\Delta z} \tag{3.1}$$

where:

N_0 is the ground refractivity (N unit) ;

z_0 is the height at the center of the change (meter);

ΔN is the total change in N (N unit);

Δz is the height range (meter) between points at which the change has reached 90 percent of its final value;

k represents the basic underlying gradient (N units/km).

By taking its first-order derivative, we have the vertical gradient dN/dz:

$$\frac{dN}{dz} = k + \frac{\Delta N}{\pi} \cdot \frac{12.63\Delta z}{\Delta z^2 + [12.63(z - z_0)]^2} \tag{3.2}$$

The profile can be customized by adjusting the parameters above. Theoretically one can generate any elevated-duct/surface-based duct profile with arbitrary inversion layer thickness and position.

3.2 Ray Tracing

Advanced Propagation Model (APM), which is a hybrid model that includes both RT and PE. It considers four different regions, each region is "dominated" by a sub-model, and each sub-model gives an optimal solution for wave propagation problem in terms of optimal trade-off between computational efficiency and accuracy [22]. In Figure 3.1, sub-models are labeled and differentiated by colors.

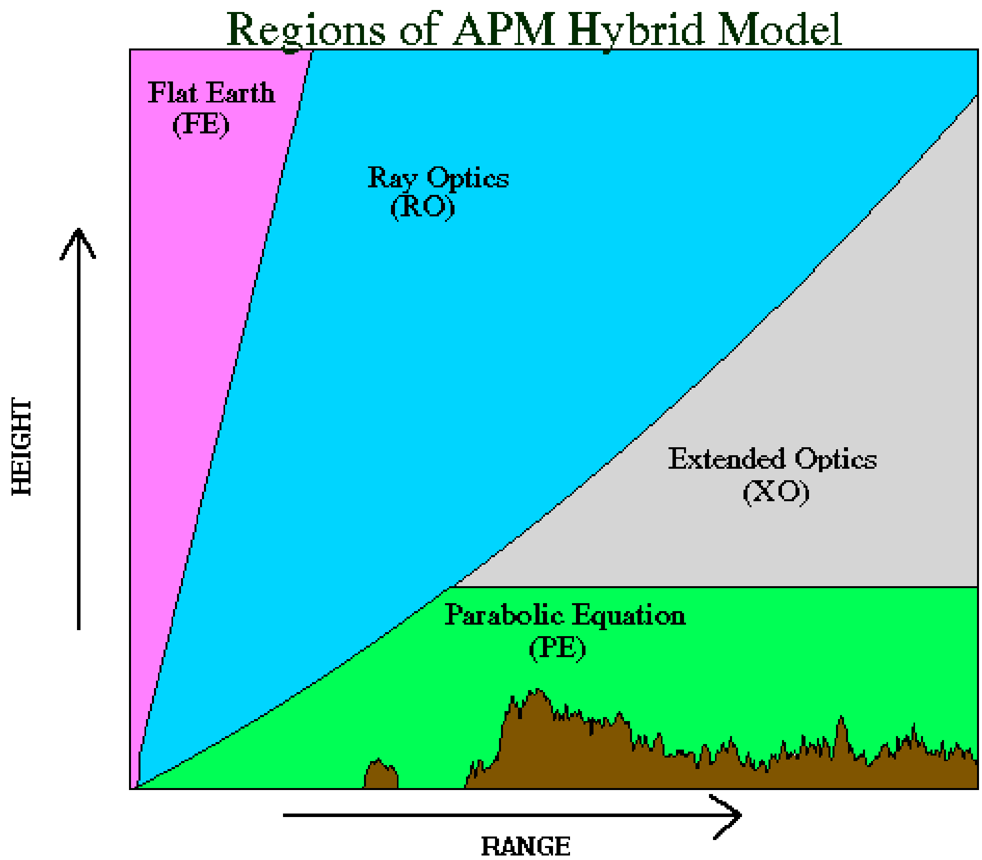

Figure 3.1: Four regions of APM [23].

APM gives good reasoning on which model to choose to solve propagation problems: the trial links concerned in this study are within the RO region because it has a hop length that is not extremely long with a small launching angle. RT model also gives a good intuitive view of ray propagation. For the region beyond the Flat Earth region where the grazing angles of reflected rays from the transmitter are above a small limiting value, a full Ray Tracing/Ray Optics model is used that accounts for the effects of refraction and earth curvature [23].

In MATLAB, a ray's initial status and nearby refractivity can be digitally written as a struct P with several fields. After the initial status is defined, ray tracing can be completed by implementing the following iterative **Algorithm 1**:

Algorithm 1 Raytracing2d

Input: A struct p_i=$\{x_i;\ y_i;\ r_i;\ \alpha_i;\ \phi_i;\ n_i\}$, defining a ray's initial status;
A struct $target$=$\{x;\ y;\ r;\ \alpha\}$, defining receiver's status;
An empty struct array $P = \{\}$, storing p from every iteration;
A double l_g, the distance ray advances in every iteration.
Output: A struct array P=$\{p_1;\ ...;\ p_{end}\}$, containing a complete path.
1: i = 1, step length = l_g
2: **while** $p_i.\alpha < target.\alpha$ **do** //stop when it hits receiver's mast
3: $\epsilon_i = \alpha_i + \phi_i$//grazing angle
4: $x_{i+1} = x_i + \sin\epsilon_i$
5: $y_{i+1} = y_i + \cos\epsilon_i$
6: $(\alpha_{i+1}, r_{i+1}) \leftarrow (x_{i+1}, y_{i+1})$ //Cartesian coordinates to radical coordinates
7: $n_{i+1} = n(r_{i+1})$ //the media is horizontally homogeneous
8: **Applying Equation 2.28**
9: **if** hitting surface **then** //assuming flat surface
10: $\phi_{i+1} = \pi - \phi_i$, **continue** from line 3
11: **else**
12: $i \leftarrow i + 1$ //moving to next direction
13: **end if**
14: Append p_i to P
15: **end while**
16: **return** P

The loop will stop when traced ray exceeds the position of receiving antenna's mast, which is represented by α_{target}.

3.3 Receiver Detection

Algorithm 1 makes sure a ray passes receiver's polar axis (antenna's mast) in radical coordinate system. To determine the exact position at which the ray hits the polar axis of the receiver, see **Algorithm 2**.

Algorithm 2 Linear interpolation

Input: A struct array P=$\{p_1;\ ...;\ p_{end};\}$, output from **Algorithm 1**;
A struct $target$=$\{x;\ y;\ r;\ \alpha\}$, defining receiver's status;
Output: A double Δh, zenith distance from point of hitting to receiving antenna.
1: $r_{interpolated} \leftarrow$ **Linear Interpolation**
2: $\Delta h = r_{interpolated} - target.r$
3: **return** Δh

3.3.1 Detection in Linear/Normal Profile

In a normal atmosphere where vertical refractivity is linearly varying with altitude, the atmosphere bends signals in only one direction. Every launching angle ϕ has a unique Δh (see **Algorithm 2**) corresponding to it (one-to-one mapping).

A mathematical technique called Small Angle Approximation, states the approximation of values of trigonometric functions given a very small angle:

$$\sin\phi \approx \tan\phi \approx \phi \tag{3.3}$$

To successfully utilize this approximation, the propagation distance of the ray must be much greater than the distance between the ray's intersection position and antenna position. In short, such a method only applies to long-range propagation scenarios.

Assuming geometric line-of-sight path as l_{geo} and detection threshold as d_{tol}, the LOS path can be found via calibrating launching angles, the calibration is provided by small-angle approximation:

Algorithm 3 Small angle approximation

Input: A struct array P={p_1; ...; p_{end};}, output from **Algorithm 1**;
A struct *target*={x; y; r; α}, defining receiver's status;
A double d_{tol}, detection threshold.
A double l_{geo}, geometric distance between two paired antennas.
Output: A double ϕ, correct launching angle.

while true do
    run Algorithm 2
    if $|\Delta h| < d_{tol}$ **then** //detected if this holds true
        break
    else
        $\phi_{new} = \phi + \frac{\Delta h}{l_{geo}}$ //calibrated launching angle
        $\phi = \phi_{new}$
    end if
    run Algorithm 1//shoot another ray with calibrated launcging angle
end while
return ϕ

The detection process will stop once the nearest iteration has Δh less than or equal to d_{tol}.

3.3.2 Detection in Multipath

In the presence of an inversion layer, a small angle approximation is no longer applicable in tracking launching angles. Depending on the layer's thickness and its refractivity gradient, multiple paths and ground reflection could happen in the same propagation medium. In this case, one Δh value could have multiple launching angles ϕ_{start} corresponding to it, simple calibration in section 3.3.1 could make launching angles deviate more and more from the desired value, leading to extremely long compiling time of programs.

A recursive algorithm called Brute Force Search (BFS) is being used in this scenario. BFS algorithm first launches a cluster of rays, each ray is evenly spaced according to specific spatial resolution, and the boundaries of such cluster are defined beforehand according antenna's radiation pattern (HPBW) exemplified in Figure A.1.

Algorithm 4 Brute Force Search

Input: A double $\Delta\phi$, antenna's HPBW;
Input: A double ϕ_{start}, geometric line-of-sight grazing angle;
Input: A double d_{tol}, detection threshold;
Input: A struct $target$={x; y; r; α}, defining receiver's status;
Input: A double res, angular separation.
Output: A double ϕ, correct grazing angle.

run Algorithm 1 and 2 for $\phi \in \{\phi_{start} - \Delta\phi : res : \phi_{start} + \Delta\phi\}$
Generate a function $\Delta h(\phi)$
if $min(|\Delta h(\phi)|) < d_{tol}$ **then** //detected if this holds true
    $\phi = \arg\min_{\phi}(|\Delta h(\phi)| - d_{tol})$
    break
else
    $y(\phi_i) = \sum_{i=1}^{N-1} \Delta h(\phi_i) \cdot \Delta h(\phi_{i+1})$ //product of adjacent elements
    $\phi_j = \arg_{\phi}(y(\phi_j) < 0)$ //extract indices that gives negative product
    $res = \frac{res}{2}$ //denser ray
    run Algorithm 4 for $\phi_{start} \in \{\phi_{j=1} : res : \phi_{j=2}\}, ..., \{\phi_{end-1} : res : \phi_{end-1}\}$
end if
return ϕ

3.4 Trapezoidal Method

The Trapezoid method numerically approximates the integration over an interval by slicing the area down into trapezoidal areas which are easier to compute, it approximates Equation 2.30 by slicing the total distance the ray travels from C_1 (source) to C_{end} (detector) into N intervals:

$$\int_{C_1}^{C_{end}} n(s)\mathrm{d}s \approx \frac{1}{2}\sum_{i=1}^{N}(s_{i+1} - s_i)[n(s_i) + n(s_{i+1})] \tag{3.4}$$

In **Algorithm 1**, ray advances an equal distance (by default MATLAB uses a spacing of 1) for every step in the propagating plane. However, in the occurrence of ground reflection or during the detection procedure, linear interpolation will be applied to the ray's segment. In those cases, the last step before the receiver or the ground will have another length. In MATLAB, one can first make arrays of n_i and of s_i respectively, then apply the trapezoid method to them. See **Algorithm 5**:

Algorithm 5 OPL

Input: A struct array P={p_1; ...; p_{end};}, output from **Algorithm 1**;
Output: A double OPL, optical path length.
1: extracting n_i and s_i from P, for $i \in \{1, end\}$
2: $OPL \leftarrow$ **Applying Trapz function**
3: **return** OPL

3.5 System Model

All possible paths (assumed number of k) between two paired antennas under inversion profile are found using **Algorithm 4** and stored in a cell array $P_{i,multipath} = \{P_1; P_2; ...; P_k\}$.

According to Equation 2.34, each MIMO sub-stream (e.g., h_{nm}) in the channel matrix (denoted by Equation 2.1) is a vector sum of multiple paths (P_i) between one TX and RX antenna pair. If only a single path is detected, $i = 1$. The total received power of a sub-stream can be calculated by taking $|h_{nm}|$, and the sub-stream phase by taking $\angle h_{nm}$.

Consequently, the total MIMO phase and related parameters (e.g., PEF in Equation 2.12) can be derived by repeating the above process for each sub-stream and applying equations in the Theory chapter.

4

Results

4.1 Simulator Verification

This section aims to verify the proficiency of the RT simulator described in Chapter 3.

4.1.1 Path Constant

Mathematically, the ray's path constant should remain constant for every step along the propagating trajectory. This is an underlying assumption for algorithms in Chapter 3 to hold. Utilizing Equation 2.21, one can numerically verify if the model is correctly implemented, see Figure 4.1.

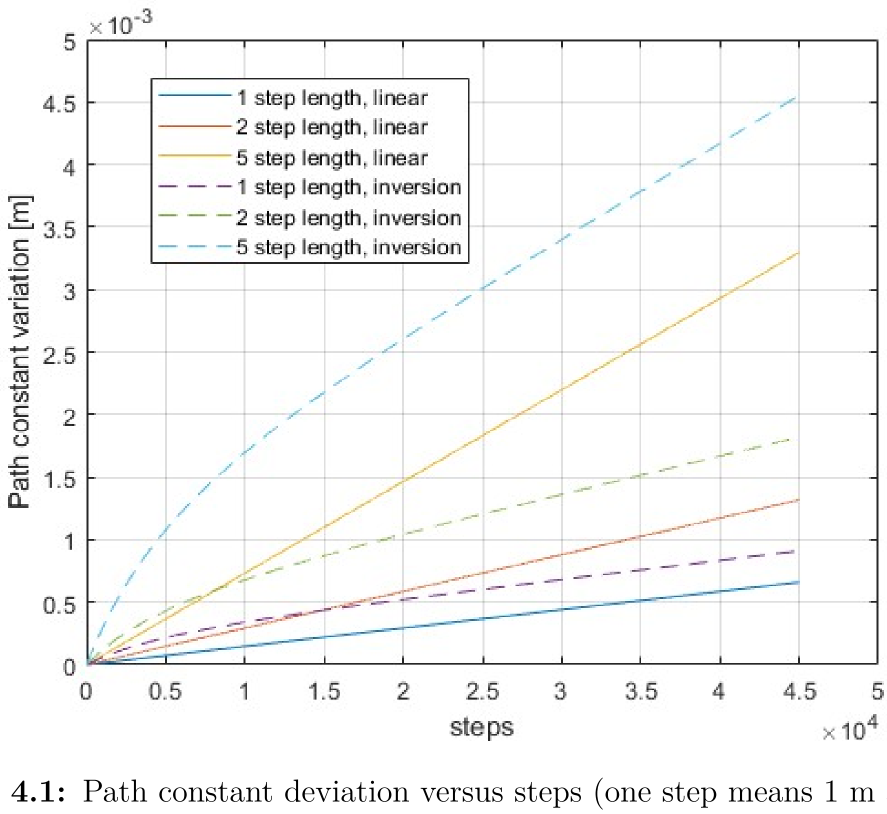

Figure 4.1: Path constant deviation versus steps (one step means 1 m advance in propagating plane), in the absence/presence of inversion layer

In Figure 4.1, the solid line indicates a linearly varying refractivity profile (referred to Figure A.2) and the dashed line indicates a profile with an inversion layer (referred to Figure A.2). It is found in both atmospheric refraction and step length (referred to **Algorithm 1**) govern the simulator accuracy. In Figure 4.1, the total variation of path constant is within 10^{-3} meter for a total of 4.5×10^4 meters propagating distance over a 2-D propagation plane, with atmospheric refractivity. Accuracy loss increases linearly in normal atmosphere conditions, whereas it has non-linear growth in the presence of an inversion layer. Larger step length also causes greater accuracy loss with the acceleration of processing time, and the inversion layer induces more accuracy loss than a normal atmosphere. A larger error was found at a longer propagating distance. To balance program running time and accuracy requirements, the simulator uses a step length of 1 m in both standard and abnormal atmosphere conditions. In the step length of 1 m, accuracy loss can be controlled within 0.1 % for a 45 km propagation distance.

4.1.2 Wave Propagation

The goal of this section is to reproduce several propagation patterns using vertical refractivity profiles mentioned in the literature. The next two cases involve only one radiation source (antenna).

The first validation (Figure 4.2) is based on Lindquist's dissertation [24], the author uses RT methods relying on the high-frequency approximation to Maxwells equations that leads to Snells law.

The refractivity profile is described as a 40 m 20 M-unit strong bilinear surface duct, at altitudes above 40 m standard atmosphere conditions apply. The transmitting antenna is placed at an altitude of 27 m. In the RT simulation rays are launched with initial angles from -0.3 degrees to 0.3 degrees in steps of 0.01 degrees [24].

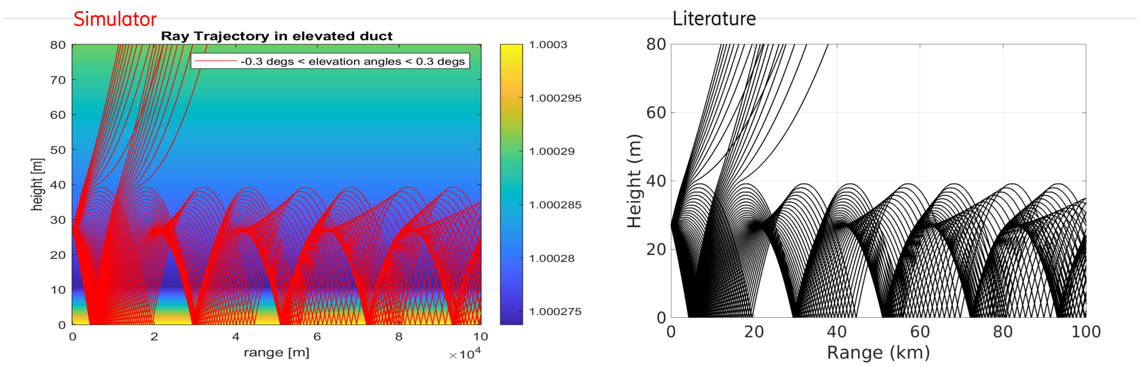

Figure 4.2: Cross validation between simulator (left) and literature [24] (right).

As shown in Figure 4.2, signals are trapped within a 40 m inversion layer and therefore they can travel very long distances. Some parts of radiated energy escape the ducting layer at propagating distances of 5 km and 15 km, similar behaviors are also observed in Lindguist's paper.

The second validation (Figure 4.3) is based on Webster's paper [13], the author uses modified Snell's law to track the wavefront's position.

An elevated duct profile was generated via Equation 3.1 and Equation 3.2. In the paper, the author sets ground refractivity N_0 to 300, basic gradient k to -39 N units/km, change in refractivity ΔN to -20 N units, height of change z_0 to 175 meters, height range of change Δz to 100 meters. The transmitting antenna was placed at 125 meters and the signal propagates over 65 kilometers distance, rays are launched with initial angles from -0.25 degrees to 0.5 degrees in steps of 0.05 degrees [13].

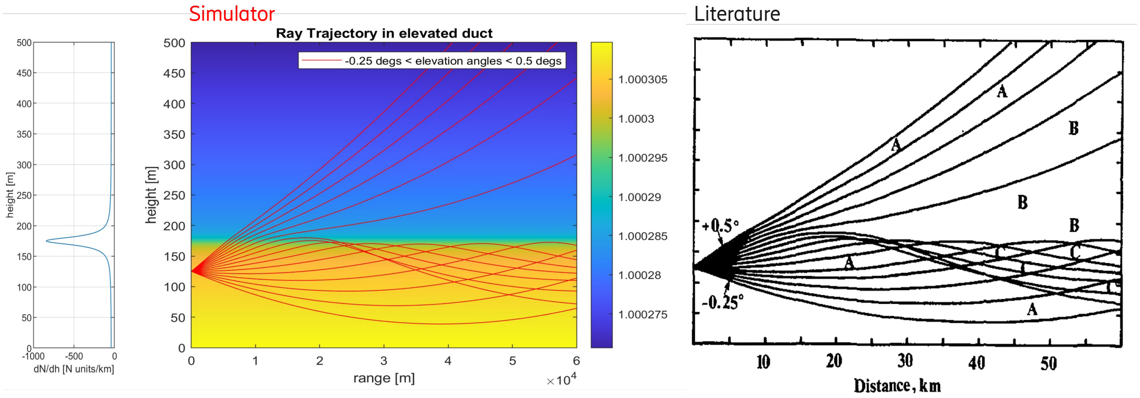

Figure 4.3: Cross validation between simulator (middle) and literature [13] (right). Figure 4.3 (middle) is the reproduced propagation pattern by the simulator in this study. The color bar to the right shows the refractivity index's distribution over the propagation space.

Figure 4.3 gives a straightforward illustration of how the atmosphere could result a multipath propagation. For those signals that travel within the elevated inversion layers (Δz) they are bent downwards, while for those that do not they just follow a curved path as they do under a normal refractivity profile.

Overall, the simulator developed in this study gives a nearly invariant path constant, and it reproduces almost identical results to those propagation patterns in other literature [13][24]. The good matches between simulation results and literature lay a solid foundation for further validation with the MIMO system using a ray tracing tool.

4.1.3 Parabolic Equation versus Ray Tracing

The goal of this section is to further verify the RT simulator used in this study by comparing its simulation results with PE's [25]. The underlying theory for the PE simulator is based on the Helmholtz Equation and its Fast Fourier Transform (FFT) numerical solution [5]. The refractivity profile parameters used in this section are shown in Table 4.1 and Table 4.2. The refractivity profiles are depicted in Figure A.2.

4.1.3.1 Standard atmosphere

The RT simulations are carried out using the same link deployment and vertical refractivity profiles as the PE-based simulation in [25]. The standard atmosphere is simulated by setting ΔN in Equation 3.2 to 0 N unit.

Table 4.1: Normal refractivity used in Figure 4.4.

ΔN	Δz	z_0	k	N_0
0 N unit	0 m	0 m	-39 N units/km	300 N unit

Lower transmitting and lower receiving antennas are placed at 59.5 m and 83.5 m respectively. The positions of the upper transmit and receive antennas will vary to verify channel conditions at different antenna separations. In Figure 4.4, antenna separation changes simultaneously on both sides by the same amount. For RT simulation, the detection threshold (d_{tol}) is 0.01 meter according to section 3.3.

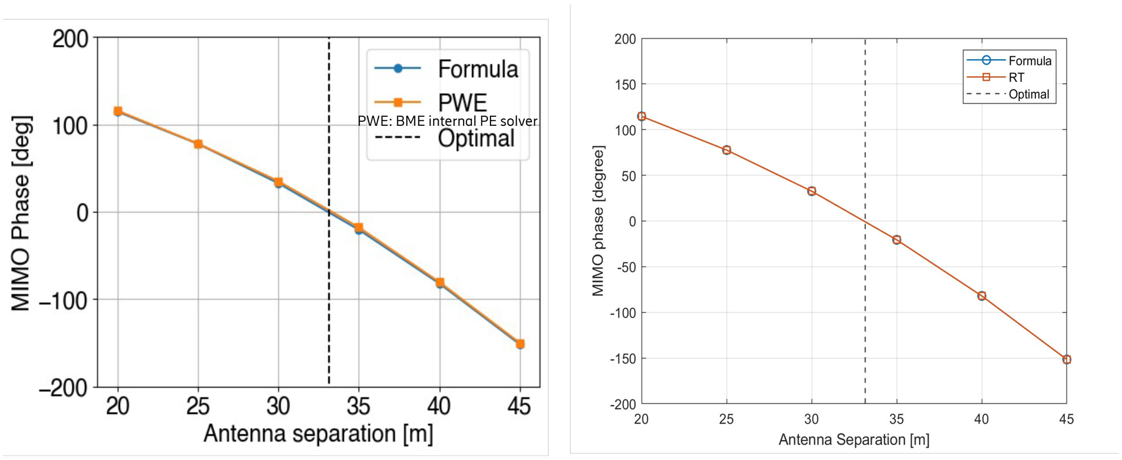

Figure 4.4: PE (left, denoted by PWE) versus RT (right), "Formula" is given by Equation 2.10. Large-value MIMO phase could cause a loss of system which leads to an outage, according to Figure 2.1.

In the standard atmosphere, both PE and RT solver are matched to the theoretical value (Formula curve) given by Equation 2.10. From the perspective of RT, the bending of the signal's trajectory is negligible in such a profile, the straight line assumption between transmit and receive antennas in a standard atmosphere is valid.

RT solver is in good agreement with the PE simulation in [25]. The results from both PE and RT simulations indicate the radio channel in a standard atmosphere behaves similarly as it does in free space conditions. RT simulator is verified in a standard atmosphere, the next step is to verify the simulator in the presence of an inversion layer.

4.1.3.2 Super refractivity

In this set of simulations, both PE and RT simulators use the same link deployment and vertical refractivity profiles. Vertical profiles are modeled by Equation 3.1, where parameters are shown in Table 4.2.

Table 4.2: Super refractivity used in Figure 4.5.

ΔN	Δz	z_0	k	N_0
-5 N unit	200 m	50 m	-39 N units/km	300 N unit

Lower transmitting and lower receiving antennas are placed at 59.5 m and 83.5 m respectively. The positions of the upper transmit and receive antennas will vary to verify channel conditions at different antenna separations. Antenna separation changes simultaneously at both sides by the same amount. For RT simulation, the detection threshold (d_{tol}) is 0.01 meter according to section 3.3.

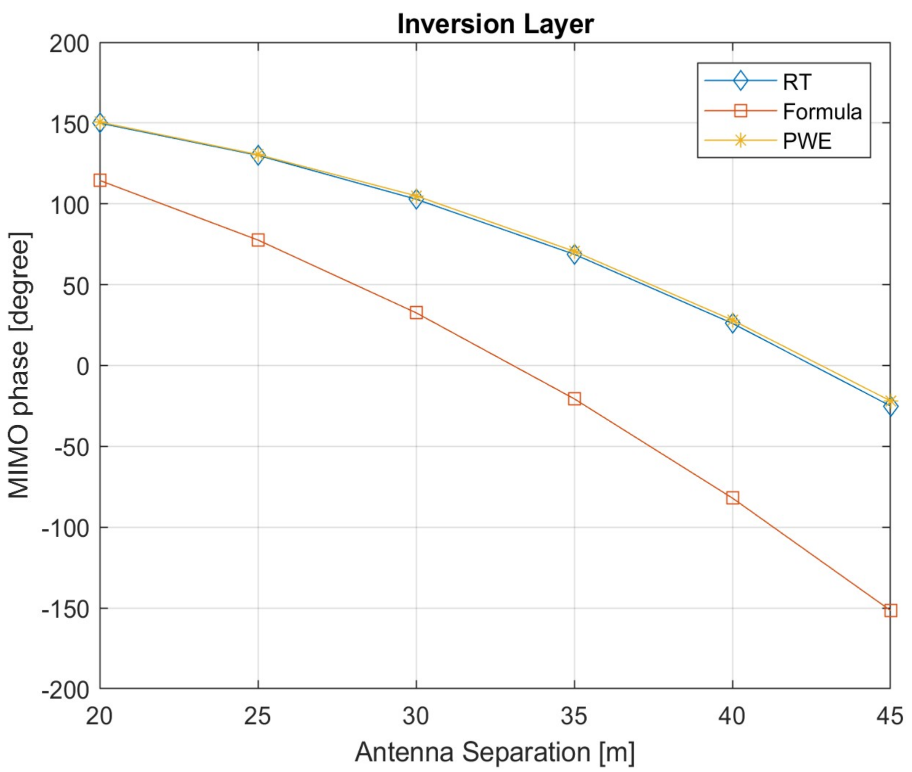

Figure 4.5: PE versus RT, "Formula" is given by Equation 2.10.

Figure 4.5 shows how the MIMO phase deviates from theoretical values (given by Equation 2.9 and Equation 2.10) as antenna separation increases with the inversion layer. As seen from the figures in this section, results from RT and PE solver are in very good agreement. For the simulated profile, the deviation in the MIMO phase from the formula case increases as increasing antenna separation. At an antenna separation of 30 m, the MIMO system with refractivity performs worse than it does without refractivity. At an antenna separation of 40 m, the MIMO system with refractivity performs better than it does without refractivity. Hence, the atmospheric refractivity can both improve or degrade the channel condition.

4.2 Super Refractivity and Ducting

In this subsection, the impact of inversion on four MIMO sub-streams and system performance under optimal antenna separation will be examined.

Abnormal refractivity is simulated by setting ΔN in Equation 3.2 to fulfill a super refractivity condition. The gradient, the thickness, and the position of the inversion layer can be controlled by adjusting parameters in Equation 3.2. The profile parameters are provided in Table 4.2. Lower transmitter and receiver antennas are at 59.5 m and 83.5 m respectively, the same as in Section 4.1. The upper transmit and receive antennas are placed optimally from the lower antennas by 33.15 m (optimal separation), the hop length is 44 km and the carrier frequency is 6 GHz. For RT simulation, the detection threshold is 0.01 meters.

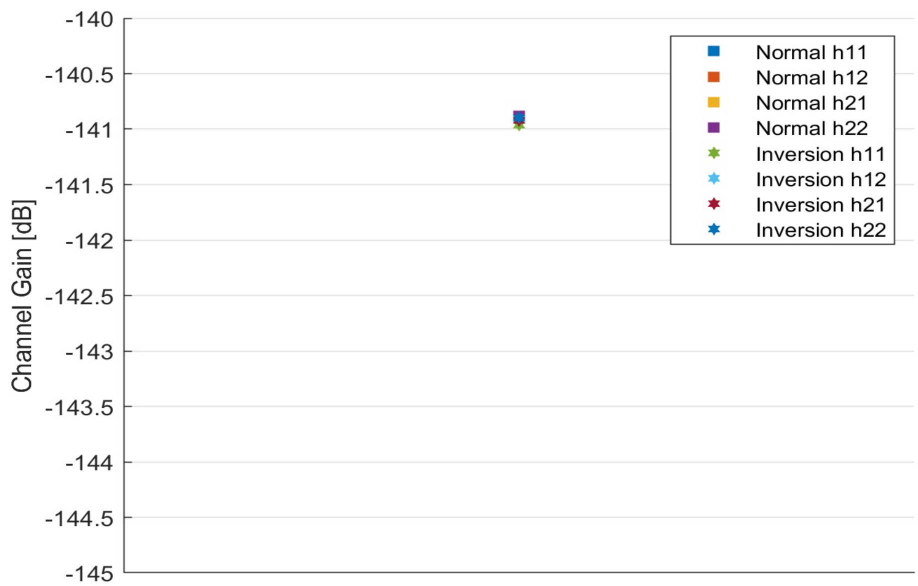

Figure 4.6: Impact of the elevated duct on channel gain of sub-streams (e.g., h_{11}), compared to the standard atmosphere. The angle of arrival and related antenna gain are considered for RX antennas, with the antenna's radiation pattern in Figure A.1.

Channel gain in Figure 4.6 is calculated for free space path loss, antenna gain relative to the main beam, and multipath fading (if exists, according to Equation 2.34). Figure 4.6 clearly shows that inversion layers from Table 4.2 do not cause much power distortion, which is always first considered when planning the microwave links. However, even if the received power is good, a big-valued MIMO phase shift may still cause an outage, as it is shown in Figure 2.1.

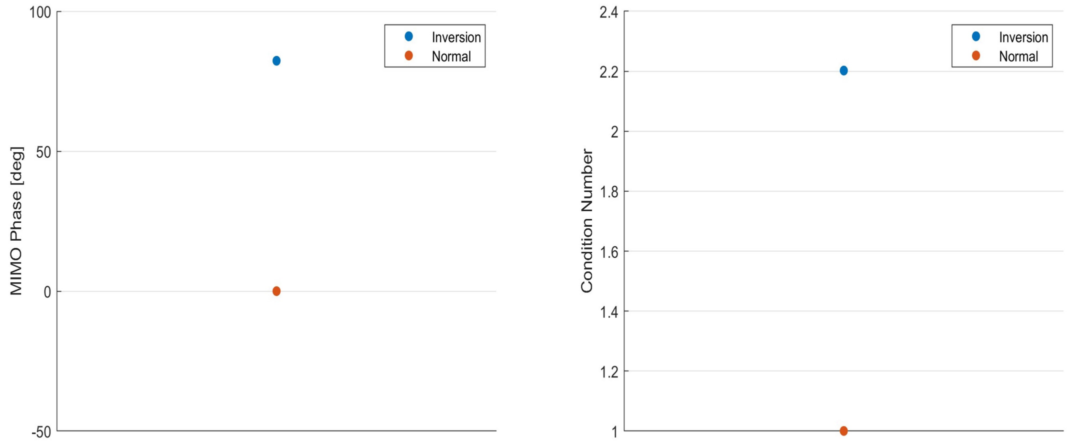

Figure 4.7: Impact of super refractivity on MIMO phase and condition number, compared to standard atmosphere.

Figure 4.7 shows the impact of the same atmospheric profile on the signal phase, using an identical experimental setup as Figure 4.6. Compared to the power variation of a single path, phase variation introduces more loss to the MIMO gain (Equation 2.12). Even for a weak super refractivity profile (ΔN = -5 N unit), a large MIMO phase shift is observed. It is expected the impact of the ducting layer (stronger than the super) on the MIMO phase is more likely to cause a system outage, as it is tested in the following simulation.

To have more insight into phase distortion caused by the inversion layer, several elevated duct profiles are generated and their impact on LOS MIMO is compared in simulation.

Table 4.3: Refractivity profiles used in Figure 4.8.

	Profile 1	Profile 2	Profile 3	Profile 4	Profile 5	Normal
ΔN (N unit)	-20	-20	-5	-5	-1	0
Δz (m)	200	100	200	100	200	0
z_0 (m)	50	50	50	50	50	0
k (N units/km)	-39	-39	-39	-39	-39	-39
N_0 (N unit)	300	300	300	300	300	300

For each profile, MIMO phases are simulated with varied antenna separation, from 20 m to 45 m and in a step of 5 m. Optimal antenna separation is marked as a dashed line for reference. The normal profile has standard refractivity with a constant vertical gradient.

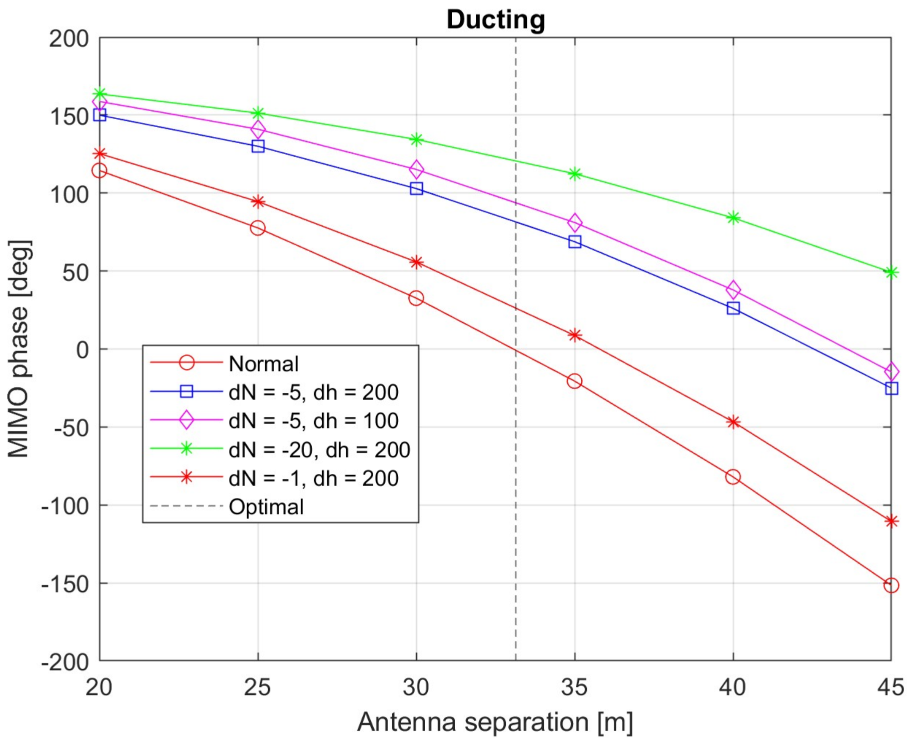

Figure 4.8: Impact of the elevated duct on MIMO phase, compared to MIMO phase in standard atmosphere.

Figure 4.8 shows how the MIMO phase deviates from the standard atmosphere (given by Table 4.1) as antenna separation increases in multiple refractivity profiles. As seen from Figure 4.8, profiles with larger ΔN and smaller Δz give greater phase shift. A strong gradient causes the signal to travel an additional optical path length, leading to extra delay/phase shift. For 20 m antenna separation, the phase shift induced by profile 1 and profile 4 are both larger than 150 degrees, MIMO system is highly likely to experience an outage according to section 2.1.6 in the Theory chapter. The position of the inversion layer also matters because one can observe strongly bent signals only if it is placed near the transmitting antenna. It is also expected similar behavior if the receive antenna is placed in an inversion layer. Whether it is placed above or below the transmitting antenna could give different results. The outage occurrence is related to both refractivity profile and antenna deployment.

One thing worth noting is, that the BFS algorithm has difficulty finding a correct path between transmitter and receiver when the atmospheric profile has ΔN of -20 N units and Δz of 100 m. This is probably because such a profile has the strongest negative gradient among all others. In such cases, no matter from what initial angle the signals were launched, they are bent straight downwards to the ground, which makes them unable to reach the receiver.

4.3 Trial Link Simulation

This section shows some simulation experiment which is based on real link deployment data and will be validated with real link measurement in a parallel project at Ericsson.

One of Ericsson's trial links is a 2x2 LOS MIMO system deployed between Uppsala and Stockholm with 44 kilometers long. This is a bi-directional link which means, each site operates both as transmitter and receiver. Similarly, each antenna is both a transmitting and receiving antenna. The link is deployed at sub-optimal antenna separation which is equivalent to 70% of optimal separation at each site.

Table 4.4: Link Setup

	Uppsala	Stockholm
Antenna size	3.7/3 m	3.7/3 m
Height (above ground level)	78.8 m/59.5 m	110.3 m/83.5 m
Height (above sea level, estimated)	100 m/120.3 m	120 m/146.8 m
Antenna Gain	45.4dBi/43.5dBi	45.4dBi/43.5dBi
Polarization	Linear(H)	Linear(H)

In the simulation setup applied here, the simulation uses the same deployment parameters as the trial link. Multiple refractivity profiles are generated by adjusting ΔN from Equation 3.2, and Δz is fixed at 120 m to have antennas covered in the inversion layer. The inversion layer has a thickness of 100 m. ΔN sweeps from 0 to 10 N units with a step size of 1 N unit, as shown in Figure 4.9.

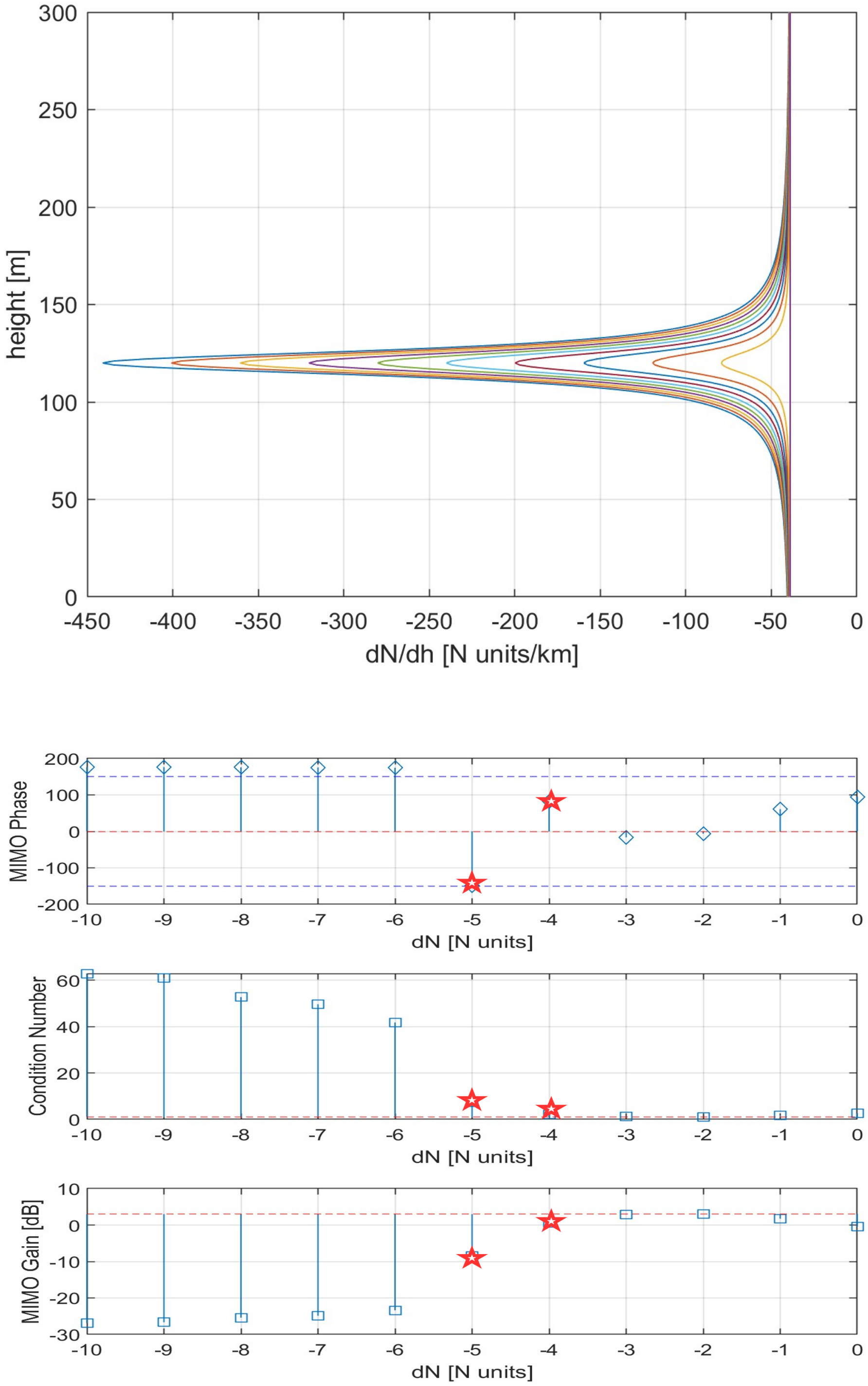

Figure 4.9: The refractivity gradient (upper) grows stronger as $|\Delta N|$ increases, and MIMO system performance (MIMO phase, condition number, MIMO gain) is simulated for each profile. The red star indicates the occurrence of atmospheric multipath (ground excluded). The Blue dashed line indicates the approximate threshold of having a system outage.

A larger MIMO phase shift (within the range [0^o 180^o]) corresponds to a larger condition number, indicating the channel is poorly conditioned. With a refractivity profile that has ΔN of -2 N units, the MIMO system has a MIMO phase and condition number closest to optimal values, indicating channel condition is optimal at this profile.

It is shown in Figure 4.9 that random phase variation (big-valued phase flip) happens for profiles that have ΔN of -5 N units and ΔN of -4 N units. Meanwhile, as they are marked with red stars in Figure 4.9, multipath is detected in these two cases. For profiles other than these two, no atmospheric multipath is observed, and the MIMO phase varies consistently with a parameter of ΔN.

5 Conclusion

This study is a step-stone toward the prediction of the availability/outage probability for MIMO links. This study developed an FRT-based propagation simulator that takes atmospheric refractivity, antenna separation, antenna radiation pattern, and ray optics into consideration.

The simulator is capable of predicting channel performance (e.g., MIMO gain, MIMO phase, channel gain, etc.) for a 2-by-2 LOS MIMO system. Total channel gain is dominated by free space path loss. Apart from free space path loss, it comprises antenna gain relative to the main beam (Figure A.1), and minor multipath fading. Free space loss and phase shift of the signal are determined by their OPL over propagation space. MIMO gain and channel gain are closely related to MIMO outage prediction, according to Figure 2.1 and Figure 2.9. To avoid an outage, Figure 2.9 demonstrates that received power should be always considered when planning an LOS microwave link. In the MIMO case, PEF should be considered as well. Figure 2.1 demonstrates the outage could still happen due to phase variation even if the received power is sufficiently good.

It is verified that the simulator has a minor accuracy loss (1 ‰) over the propagation distance concerned in this study. However, it has either linear or non-linear loss of accuracy over distance, depending on the refractivity profile. By what it is tested for so far, the simulator is capable of producing similar propagation patterns in literature for distances up to 100 km. In cases studied in this thesis, the FRT-based simulator is capable of producing almost identical results as a PE model in terms of predicting the MIMO phase.

The simulator does not consider the terrain roughness and terrestrial objects, nor their impact on electromagnetic waves. For ground reflection in Figure 4.2, the reflected ray comes from planar reflection [26]. In the general case, microwave link planning will ensure that there is little reflected path entering the receiving antenna.

The simulator is tested for varying LOS MIMO antenna separation, from optimal deployment to close antenna separation. Additionally, the simulator is tested for vacuum, linear/piecewise linear refractivity profiles, and refractivity profiles with an inversion layer, with fixed antenna separation. The study found:

- In a standard atmosphere, a 2x2 line-of-sight MIMO system behaves almost identically as it does in the free space condition. This conclusion holds for a link that has a hop length (45 km) deployed by Ericsson.

- In ducting and super refractivity, the inversion layer can cause both power and phase distortion to the propagated signal. However, the MIMO system could have an outage more likely due to the big-valued phase shift induced by atmosphere activities.

- For sub-optimal deployment, the atmospheric refractivity may improve the channel condition.

- The atmospheric multipath may induce random MIMO phase variation.

This study provides insight into how atmospheric refractivity affects LOS MIMO links, which has been rarely studied before. The FRT-based simulator shows good potential for future validation studies of real link measurements. It can also be used in supporting the development of the availability model of the LOS MIMO system. It is possible to extend the current simulator to higher-order LOS MIMO systems with arbitrary numbers of dual-polarized transmit and/or receive antennas.

The validation with real link measurement has its research challenges. On the one hand, existing temperature, humidity, and air pressure sensors operate with extremely low sampling frequency, which gives meteorological data of low temporal and spatial resolution. Therefore, the synchronization and resolution match between meteorological data and MIMO link measurement data would be a challenge. On the other hand, there has been very little literature that has strong relevance to this study.

This is an important and rarely explored research area, and the author suggested some successive work that can be further looked into.

5.1 Future Work

The following areas can be explored as potential future work:

- **Advanced Channel Modeling:** The thesis primarily focused on vertical atmosphere (horizontally homogeneous) models for simulations. However, further investigation can be conducted to refine these models and incorporate additional factors such as non-homogeneous media, air turbulence, etc.

- **Experimental Validation:** While simulations provide quantitative results, real-world measurements can validate the quantitative results of the thesis. Field trials can be performed in different geographical locations and weather conditions to assess the accuracy and limitations of the model.

- **Peer Review:** Given the same experimental setup and atmosphere model, a full comparison between the solutions by RT and those by PE can be used to verify the proficiency/reliability of the simulator, since only the MIMO phase is cross-validated in this study.

- **Terrain Roughness:** The thesis mainly focused on developing a pure atmosphere propagation model. However, terrain conditions also play an important role in affecting wave propagation. In reality, irregular terrain and surface objects (e.g. foliage) interact with electromagnetic waves variously, signals will be scattered, diffracted, and so on. An advanced ground modeling, e.g., staircase method and PLSM (Piecewise Linear Shift Map) method [24], is needed to combine with FRT to give a more accurate prediction on wave behaviors.

Bibliography

[1] I. Tryggvi and H. Liu, "Line-of-sight MIMO for microwave links: adaptive dual polarized and spatially separated systems," Master of Science Thesis, Chalmers University of Technology, Sweden, July 2009.

[2] International Telecommunications Union (ITU-R), "Propagation data and prediction methods required for the design of terrestrial line-of-sight systems," Recommendation ITU-R P.530-18, 2021.

[3] P. Eriksson, S. A. Buehler, C. P. Davis, C. Emde, and O. Lemke (2011), ARTS, the atmospheric radiative transfer simulator, Version 2, J. Quant. Spectrosc. Radiat. Transfer, doi:10.1016/j.jqsrt.2011.03.001.

[4] Z. Carneil. (2023). "Parabolic equation models simulating LoS MIMO conditions (Dissertation)." Retrieved from https://urn.kb.se/resolve?urn=urn:nbn:se:kau:diva-96366

[5] G. Apaydin and L. Sevgi, "The Split-Step-Fourier and Finite-Element-Based Parabolic-Equation Propagation-Prediction Tools: Canonical Tests, Systematic Comparisons, and Calibration," in IEEE Antennas and Propagation Magazine, vol. 52, no. 3, pp. 66-79, June 2010, doi: 10.1109/MAP.2010.5586576.

[6] K. Rundstedt, L. Bao, R. Krishnan, B. -E. Olsson and T. Eriksson, "On Field Measurements and Modelling of 2x2 Microwave LOS-MIMO Systems," 2015 IEEE Global Communications Conference (GLOBECOM), San Diego, CA, USA, 2015, pp. 1-6, doi: 10.1109/GLOCOM.2015.7417256.

[7] A. Goldsmith, Wireless communications, Cambridge university press, 2005.

[8] C. B. Papadias, Chapter 11 - MIMO communication for wireless networks, Editor(s): Sarah Kate Wilson, Stephen Wilson, Ezio Biglieri, Academic Press Library in Mobile and Wireless Communications, Academic Press, 2016, Pages 399-433, ISBN 9780123982810, https://doi.org/10.1016/B978-0-12-398281-0.00011-9.

[9] L. Bao and B. -E. Olsson, "Methods and measurements of channel phase difference in 2x2 microwave LOS-MIMO systems," 2015 IEEE International Con-

ference on Communications (ICC), London, UK, 2015, pp. 1358-1363, doi: 10.1109/ICC.2015.7248512.

[10] R. Zhang, S. Zhang, Z. Zhao, Z. Wu, C. Lu and L. Lin, "Phase Turbulence Prediction Method for Line-of-Sight Multiple-InputMultiple-Output Links Caused by Atmospheric Environment," in IEEE Antennas and Wireless Propagation Letters, vol. 21, no. 9, pp. 1867-1871, Sept. 2022, doi: 10.1109/LAWP.2022.3183439

[11] LCDR Bruce W. Ford. Atmospheric Refraction: How Electromagnetic Waves Bend in the Atmosphere and Why It Matters.

[12] Z. Kaymaz., and Mentes, , 2007: "Investigation of Surface Duct Conditions over Istanbul, Turkey." J. Appl. Meteor. Climatol., 46, 318337, https://doi.org/10.1175/JAM2452.1.

[13] A. Webster, "Raypath parameters in tropospheric multipath propagation," in IEEE Transactions on Antennas and Propagation, vol. 30, no. 4, pp. 796-800, July 1982, doi: 10.1109/TAP.1982.1142840.

[14] International Telecommunications Union (ITU-R), "Attenuation by atmospheric gases and related effects," Recommendation ITU-R P.676-10, 2013.

[15] C. Rodgers, "Inverse methods for atmospheric sounding: Theory and practise," 1st ed., World Scientific Publishing, 2000.

[16] F.A. Jenkins and H.E. White, (1981) "Fundamentals of Optics. 4th Edition," McGraw-Hill.

[17] J. E. Hasbun; "On the optical path length in refracting media. " American Journal of Physics 1 April 2018; 86 (4): 268274. https://doi.org/10.1119/1.5013008

[18] D. Minoli, (2009) Satellite Systems Engineering in an IPv6 Environment (1st ed.). CRC Press. Retrieved from https://www.perlego.com/book/1603173/satellite-systems-engineering-in-an-ipv6-environment-pdf (Original work published 2009)

[19] D. Large, J. Farmer, Chapter 6 - Linear Microwave Signal Transportation, Editor(s): David Large, James Farmer, In The Morgan Kaufmann Series in Networking, Broadband Cable Access Networks, Morgan Kaufmann, 2009, Pages 161-184, ISSN 18759351, ISBN 9780123744012

[20] M. Holker, 27 - Radiowave propagation, Editor(s): Fraidoon Mazda, Telecommunications Engineer's Reference Book, Butterworth-Heinemann, 1993, Pages 27-1-27-15, ISBN 9780750611626, https://doi.org/10.1016/B978-0-7506-1162-6.50033-2.

[21] D. M. Dobkin, Chapter 4 - UHF RFID Readers, Editor(s): Daniel M. Dobkin,

The RF in RFID (Second Edition), Newnes, 2013, Pages 103-188, ISBN 9780123945839, https://doi.org/10.1016/B978-0-12-394583-9.00004-1.

[22] J. Derksen, (2016). "Radar Performance Modelling; A study of radar performance assessment accuracy to the resolution of atmospheric input data." Case studies of North Sea environments.

[23] A. E. Barrios, "Considerations in the development of the advanced propagation model (APM) for U.S. Navy applications," 2003 Proceedings of the International Conference on Radar (IEEE Cat. No.03EX695), Adelaide, SA, Australia, 2003, pp. 77-82, doi: 10.1109/RADAR.2003.1278714.

[24] T. Lindquist, (2020). "Wave Propagation Models in the Troposphere for Long-Range UHF/SHF Radio Connections (Dissertation)." Retrieved from http://urn.kb.se/resolve?urn=urn:nbn:se:kau:diva-80679

[25] B. Horvath and P. Horvath, "Status report on Development of availability simulator/model for LOS-MIMO microwave links in tropospheric propagation channel," Internal report, Budapest University of Technology and Economics, June 2023

[26] Z. Yun and M. F. Iskander, "Ray Tracing for Radio Propagation Modeling: Principles and Applications," in IEEE Access, vol. 3, pp. 1089-1100, 2015, doi: 10.1109/ACCESS.2015.2453991.

A

Appendix 1

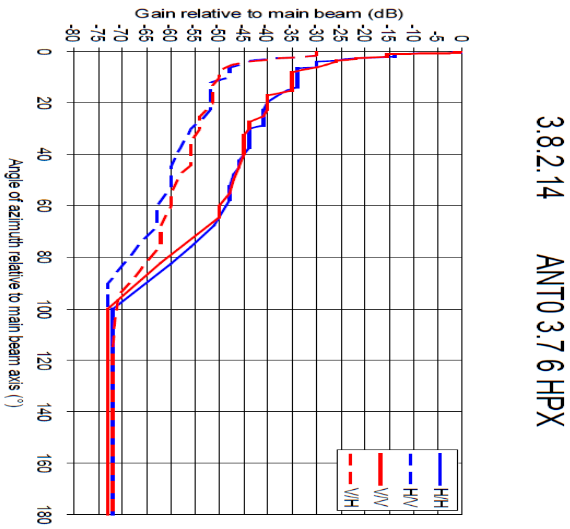

Angle (°)	H/H (dB)	Angle (°)	H/V (dB)	Angle (°)	V/V (dB)	Angle (°)	V/H (dB)
0.00	0.00	0.00	-30.00	0.00	0.00	0.00	-30.00
0.11	-0.07	1.50	-30.00	0.10	-0.03	1.50	-30.00
0.20	-0.37	2.50	-38.00	0.20	-0.41	2.50	-38.00
0.30	-0.95	3.50	-44.00	0.30	-0.95	3.00	-38.00
0.40	-1.90	5.00	-46.00	0.40	-1.73	4.00	-44.00
0.50	-3.08	6.00	-48.00	0.49	-2.84	5.00	-47.50
0.60	-4.64	10.00	-48.00	0.60	-4.47	7.50	-50.00
0.70	-6.57	12.00	-52.00	0.70	-6.19	10.00	-50.00
0.80	-8.90	22.50	-52.00	0.80	-8.36	13.00	-51.50
0.90	-12.00	27.00	-54.00	0.88	-11.03	15.00	-51.50
0.96	-14.00	30.00	-56.00	1.00	-15.50	20.00	-51.50
1.80	-14.00	37.50	-58.00	2.00	-15.50	25.00	-54.00
2.00	-14.00	44.50	-60.00	2.50	-22.00	30.00	-54.00
2.50	-22.00	52.50	-60.00	3.00	-22.00	35.00	-56.00
3.00	-24.00	60.00	-63.00	3.50	-26.00	44.00	-56.00
3.50	-26.00	67.50	-63.00	4.00	-26.00	47.50	-58.00
4.00	-30.00	75.00	-66.50	5.00	-28.00	55.00	-60.00
5.00	-30.00	90.00	-73.00	6.00	-30.00	60.00	-60.00
6.00	-30.00	180.00	-73.00	7.00	-33.00	67.50	-62.00
6.50	-34.00			8.00	-35.00	75.00	-62.00
7.50	-34.00			10.00	-35.00	84.50	-66.00
10.00	-34.00			15.00	-35.00	95.00	-71.00
14.00	-34.00			17.00	-40.00	115.00	-72.00
15.00	-36.00			20.00	-40.00	180.00	-72.00
16.50	-37.50			22.50	-40.00		
19.50	-40.00			25.00	-41.00		
22.50	-41.00			27.50	-44.00		
28.50	-41.00			30.00	-44.00		
30.00	-44.00			32.50	-45.00		
37.50	-44.00			40.00	-45.00		
42.50	-46.00			45.00	-46.00		
45.00	-46.00			50.00	-47.00		
47.50	-47.00			55.00	-48.00		
52.50	-48.00			60.00	-50.00		
57.50	-48.00			64.50	-50.00		
67.50	-51.00			82.00	-62.00		
76.00	-56.00			100.00	-73.00		
82.50	-60.00			180.00	-73.00		
100.00	-72.00						
180.00	-72.00						

Figure A.1: Antenna's radiation pattern, 3.7 m diameter dish, 6 GHz operating frequency

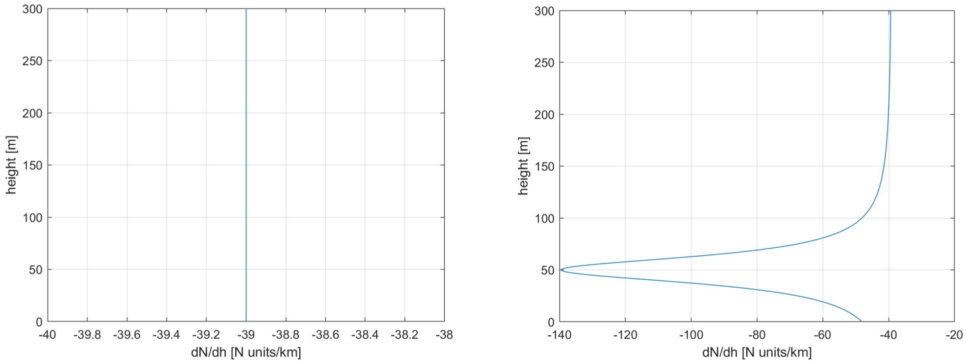

Figure A.2: Standard atmosphere(left) generated by Table 4.1, super refractivity (right) generated by Table 4.2.

DEPARTMENT OF SOME SUBJECT OR TECHNOLOGY
CHALMERS UNIVERSITY OF TECHNOLOGY
Gothenburg, Sweden
www.chalmers.se

CHALMERS
UNIVERSITY OF TECHNOLOGY